

# Modelling aboveground biomass of a multistage managed forest through synergistic use of Landsat-OLI, ALOS-2 L-band SAR and GEDI metrics

Hitendra Padalia <sup>\*</sup>, Ankit Prakash, Taibanganba Watham

*Forestry and Ecology Department, Indian Institute of Remote Sensing, Indian Space Research Organisation Dehradun, 248001, India*



## ARTICLE INFO

**Keywords:**

Canopy height  
Himalaya  
LiDAR  
GEDI  
RADAR

## ABSTRACT

To better understand forest carbon budgets and design forest-based climate change mitigation solutions, reliable biomass estimation is critical. Integrating multi-sensor remote sensing data can improve forest monitoring and evaluation. This study adopted a one-hectare plot size sampling design to improve the integration of GEDI footprints with in-situ, optical, and SAR data for the estimation of forest above-ground biomass (AGB). The study was carried out for a managed tropical forest in the Himalayan foothills of India. The space-borne GEDI retrieved the canopy height of the study area with an RMSE of 3.36 m and Adj. R<sup>2</sup> of 0.70. Extrapolating GEDI footprint heights (RH95) with Landsat 8 indices using Random Forest (RF) yielded a spatial canopy height of the study area with an R<sup>2</sup> of 0.97 and RMSE of 2.32 m. Using the GEDI canopy height, foliage density, and plant area index, the AGB at GEDI footprints level was estimated using RF, with an R<sup>2</sup> of 0.91 and an RMSE of 20.10 Mg ha<sup>-1</sup>. The spatial AGB model that only considered ALOS-2 SAR variables had an R<sup>2</sup> of 0.61 and an RMSE of 18.27 Mg ha<sup>-1</sup>, whereas the RF model that considered both SAR variables and canopy height had a superior R<sup>2</sup> of 0.77 and a lower RMSE of 13.86 Mg ha<sup>-1</sup>. The addition of canopy height data reduced the RMSE of the AGB model by 4.41 Mg ha<sup>-1</sup> and also predicted a higher range of AGB. The study demonstrates the effectiveness of combining GEDI data with other sensors (optical and SAR data) to provide precise AGB of multistage managed forests using a one-hectare plot size sampling design.

## 1. Introduction

Accurate monitoring of forest biomass and CO<sub>2</sub> sequestration rates is vital for improving knowledge of the carbon cycle while offering critical information for climate change mitigation and adaptation measures (Gibbs et al., 2007; Way and Pearcy, 2012). Forest biomass is traditionally calculated from field measured diameter and height of trees using a species-specific volume table or equation, which is expensive and spatially limiting (Boisvenue et al., 2016; Hyppa et al., 2000). Remote sensing has emerged as the most popular method for estimating forest above-ground biomass (AGB) across various scales, from landscapes to regions and even continents, due to its repeatability, cost-effectiveness, and global coverage (Herold et al., 2019; Masek et al., 2015; Mauya et al., 2019).

Optical remote sensing provides information on horizontal vegetation structures such as cover, type, and density (Chrysafis et al., 2019; Kilpeläinen and Tokola, 1999; Lausch et al., 2017), but it offers limited information on tree height and vertical structure where the greatest biomass is concentrated (Olesk et al., 2016). However, optical remote

sensing had been utilised to quantify forest AGB at various spatial and temporal scales using various image-processing approaches (Lu, 2005; Zheng et al., 2004). Clouds, smoke, and bad illumination hinder optical remote sensing, and optical sensor-based AGB estimate suffer from significant saturation issues (Hyppa et al., 2000).

Another well-known technique for AGB estimation is the use of all-weather active microwave sensors, such as Synthetic Aperture Radar (SAR), with better penetrability and vertical information derived from different frequency bands, polarisations, and imaging geometries (Chen et al., 2021; Lausch et al., 2017). Longer wavelengths (i.e., L- and P-band) SAR are promising technology for the estimation of forest AGB (Yu and Saatchi, 2016). Currently, ALOS-2 (Advanced Land Observing Satellite) is the main source of L-band SAR data. Future L-band (NISAR, TanDEM L, ALOS-4) and P-band (BIOMASS) SAR satellite missions will provide consistent longer wavelength SAR data for global carbon investigation. The empirical relationship between SAR backscatter and field-measured AGB is the most common method for AGB estimation (Ghasemi et al., 2011). However, in closed heterogeneous forests, SAR experiences signal saturation when volume exceeds 200 m<sup>-3</sup> ha<sup>-1</sup> (Santi

\* Corresponding author.

E-mail address: [hitenpadalia@gmail.com](mailto:hitenpadalia@gmail.com) (H. Padalia).

et al., 2015; Zhang et al., 2020). In addition to SAR backscatter, two-wavelength interferometry (Balzter, 2001; Balzter et al., 2007; Saatchi et al., 2011), the water cloud model (WCM) (Cartus et al., 2012; Khati et al., 2021; Kumar et al., 2012), and the random volume over ground (RoVG) model (Hajnsek et al., 2009; Mette et al., 2004; Yadav et al., 2021) are different approaches used in forest AGB estimation. Yet, the universal application of these physical inversion models for AGB estimation of large geographic regions and complicated topography requires demonstration.c.

Over the past few years, Light Detection and Ranging (LiDAR) has demonstrated significant potential for mapping forest canopy height (Lefsky et al., 2002) while minimizing saturation issues (Cartus et al., 2012; Puliti et al., 2018). Canopy height may be accurately measured using aerial LiDAR. However, it is too expensive to utilize throughout space and time. As a result, it has only been used in a few locations, mostly in the tropics (Asner et al., 2012). Space-based LiDAR data is a viable alternative source of information for improving forest AGB estimates from regional to global scales (Baccini et al., 2012). However, due to a lack of spatial consistency, LiDAR data are still used as a supplementary data in forest AGB mapping (Chen et al., 2021).

Biomass maps have been improved using data from the Ice, Cloud, and Land Survey Satellites (ICESat)-Geoscience Laser Altimeter System (GLAS) LiDAR (Harding et al., 2001; Popescu et al., 2011; Simard et al., 2011). Improved estimates of canopy height and AGB have been achieved using ATLAS (Advance Topographic Laser Altimeter System) point clouds LiDAR onboard ICESat-2 (Narine et al., 2020) and GEDI's LiDAR waveform (Potapov et al., 2021). GEDI LiDAR data from space can be used to estimate forest stand heterogeneity and associated tree species diversity in forest ecosystems (Torresani et al., 2023). Ni-Meister et al. (2022) used a waveform/foliage profile-weighted height-based allometric equation to directly estimate plot-level AGB from large-footprint waveform LiDAR. They discovered that, except for boreal forests, a single generic model performs rather well across all worldwide forest biomes.

In ecological study, data integration is frequently considered necessary, as processes and patterns of interest are the outcomes of interactions between complex physical phenomena (Schildhauer, 2018). Integrating multi-sensor remote sensing data can improve forest monitoring and evaluation (Lehmann et al., 2015; Mauya et al., 2019). Hyde et al. (2006) investigated the feasibility of combining information from several sensors to generate forest structure and found the best single sensor for predicting canopy height and AGB is LiDAR, with an RMSE of 8.8 m (InSAR RMSE of 11.9 m, ETM RMSE of 9.6 m). Chen et al. (2012) increased the accuracy of the AGB estimate by combining LiDAR data with plant-type information. The  $R^2$  statistic increased from 0.77 to 0.83, and the RMSE decreased by 10% (from 80.8 to 72.2 Mg ha $^{-1}$ ). The combined use of LiDAR and SAR data improves AGB estimation accuracy (Mitchard et al., 2012; Montesano et al., 2014; Qi et al., 2019). Nandy et al. (2021) found that integrating canopy height information with spectral information acquired from optical data increased the performance of the AGB model in their investigation of the Himalayan foothill forest. They produced a forest height map based on an RF model with  $R^2$  of 0.84, RMSE of 1.15 m, and %RMSE of 4.48% using ICESat-2 LiDAR and C-band Sentinel-1 data.

For biomass modelling, statistical and machine learning approaches are generally used to predict AGB by integrating diverse remote sensing datasets with field data. However, machine-learning models outperform the parametric linear model by lowering the degree of saturation (Hojo et al., 2023). Shendryk (2022) used gradient-boosting ensemble decision trees to fuse GEDI, Sentinel-1, Sentinel-2, elevation, and land cover data for large-scale AGB mapping with  $R^2$  of 0.66–0.74, RMSE of 55–81 Mg ha $^{-1}$ , and RMSE% of 41–77% for forested lands equivalent to 9.8 Pg and 37.1 Pg in Australia and the United States, respectively.

Dhanda et al. (2017) used RF regression approach based on ICESat/GLAS and high-resolution optical data to estimate the AGB of a sal forest in India, with an  $R^2$  of 0.83 and RMSE of 20.57 Mg ha $^{-1}$ . Chi et al. (2015)

used the RF algorithm to map China's AGB using GLAS/ICESat LiDAR, MODIS data, and forest inventory data. More frequently than not, studies has demonstrated greater accuracy with multi-sensor data integration approach (Li et al., 2020; López-Serrano et al., 2020; Nandy et al., 2021; Wu et al., 2016; Zhang et al., 2020).

The United Nations programme to reduce emissions from deforestation and forest degradation (REDD) recommends that biomass estimates errors be kept to less than 20 Mg ha $^{-1}$ , but should not exceed 50 Mg ha $^{-1}$  (Hall et al., 2011; Houghton et al., 2009). GEDI's Level 1 scientific output estimates AGB of 80% of 1 km cells within a standard error of 20 Mg ha $^{-1}$  or 20% of the estimate, whichever is lesser (Dubayah et al., 2022). The planned NISAR mission seeks to estimate AGB within 20 Mg ha $^{-1}$  RMSE for forests with AGB density of less than 100 Mg ha $^{-1}$  (NISAR Science Team, 2019).

There are several challenges in integrating multisource satellite data with field measured AGB. Addressing the field-of-view discrepancy is one of the major problem when merging observations from multiple equipment (Dubovik et al., 2021). Even when the plot size is altered based on satellite data for AGB calculation, difficulty in determining the precise position of the plot inside the forest owing to GPS inaccuracy is frequent (Réjou-Méchain et al., 2019). Similarly, the LiDAR footprint does not always correspond to the actual dimensions of the trees, resulting in disparity between field inventory data and satellite data. The reported range of horizontal co-registration precision for GEDI is 6.5 m to 10.3 m (Dubaya, 2021; Luthcke et al., 2019; Sun et al., 2022). Due to geolocation uncertainty, high interquartile values more than or equivalent to relative height (RH) are found at the GEDI footprint site of spatially diverse canopies, including canopies with limited forest stands, gaps in the plant canopy, and forest edges.

GEDI's geolocation uncertainty is a well-known problem which must be addressed when utilising GEDI in combination with other satellite data (Roy et al., 2021). A bigger plot size would be beneficial to decrease the effect of GPS inaccuracies and edge effects. Larger plot sizes are expected to lower model error owing to so-called spatial averaging error, because larger plot sizes capture more geographical variation in both, field observations and satellite data (Mauya et al., 2015). Therefore, this study is based on a one-hectare (ha) sample plot in order to improve the integration of GEDI footprints with in-situ, optical, and SAR data.

The study area consists of multi-age stands with a wide range of canopy heights and AGB. SAR interferometry may be used to obtain canopy height. However, to successfully capture the canopy height, multiple InSAR observations with distinct baselines and wave number pairs are required (Yadav et al., 2021). The effective vertical wave number is critical in establishing forest height through SAR interferometry (Ahmed et al., 2011), and the range of vertical wave number is limited when inverting the forest height using the RVoG model (Kugler et al., 2015). Therefore, LiDAR is the ideal choice for retrieving canopy height information, which can then be included into AGB modelling for precise AGB estimates. GEDI LiDAR-based canopy height modelling is essential at the local level since global canopy height models use biome and climatic data to extrapolate canopy height across the landscape (Potapov et al., 2021).

The objective of present research is to integrate GEDI data with Landsat 8 and ALOS-2 L-band SAR images to estimate the AGB of managed tropical forests in the Terai Central Forest Division in the foothills of the North West Himalayas. The sub-objectives are to (i) estimate spatial canopy height using optimum GEDI RH and Landsat 8-derived indices; (ii) estimate the AGB of GEDI ground tracks of 1-ha plots using field sample AGB and corresponding GEDI metrics; (iii) estimate the AGB of the study area using ALOS-2 L-band SAR data at the appropriate time and compute associated uncertainty; and (iv) estimate the AGB of the study area by combining canopy height and SAR variables and compute associated uncertainty.

## 2. Materials and methods

### 2.1. Study area

The study area is Terai Central Forest Division (TCFD) in Nainital district of Uttarakhand state (India) (Fig. 1), and it is located between  $29^{\circ}01'30''$  to  $29^{\circ}16'40''$  north latitude and  $79^{\circ}13'45''$  to  $79^{\circ}00'31''$  east longitude. The TCFD comprises of seven forest ranges: Barhani, Bhakra, Gadgadia, Haldwani, Peepalpadao, Rudrapur, and Tanda, with a total area of 40,496 ha (Uttarakhand Forest Department, 2016). The entire research area has a fairly gradual slope from the northern Bhabar region to the southern Terai region. The soil type is alluvial loam to sandy loam. The climate is tropical humid, and the annual rainfall in the study region is around 1100 mm (Watham et al., 2021), with more than 80% of the rainfall occurring between July and September. The site is mostly composed of monocultures plantation of *Eucalyptus* spp., *Tectona grandis*, and *Populus deltoides*, with some mixed plantings of native deciduous tree species such as *Acacia catechu*, *Mallotus philippensis*, *Trewia nudiflora*, *Cassia fistula*, *Dalbergia sissoo*, and *Holoptelea integrifolia*. The stand density in mixed plantations is 350–450 trees  $\text{ha}^{-1}$ , the age range is highly variable, ranging from 5 to 50 years. The harvesting age of *Eucalyptus* spp. and *Populus* spp. varies between 10 and 15 years, with stand density ranging between 600 and 800 trees  $\text{ha}^{-1}$ . Meanwhile, the harvesting age for teak is above 40 years, with a stand density of 300–400 trees  $\text{ha}^{-1}$ , and the current age range is 15–50 years. The plantation blocks are larger than 3 ha in size and planted at varied intervals (Padalia and Yadav, 2016).

### 2.2. Datasets

#### 2.2.1. GEDI data

The GEDI LiDAR onboard the International Space Station (ISS) started data collection on December 5, 2018 and gathers data between  $51.6^{\circ}\text{N}$  and  $51.6^{\circ}\text{S}$ . It consists of three lasers that produce eight ground transects with a footprint resolution of 25 m spaced 60 m along-track and 600 m across-track the orbit with an overall width of 4.2 km on the ground. Two of the three lasers are full-power lasers, while one is a coverage laser. The GEDI product includes the complete waveform (raw data), elevation, height metrics, and vegetation biophysical traits (Dubayah et al., 2020). GEDI L2A (elevation and height measurements) and L2B (plant area index (PAI), foliage cover, foliage height diversity

(FHD), and canopy gap data sets were downloaded from LPDAAC (Land Processes Distributed Active Archive Centre) from April 2019 to August 2020 (<https://lpdaac.usgs.gov>).

#### 2.2.2. Landsat 8 data

Landsat 8 OLI (Operational Land Imager), which was launched on February 11, 2013, captures data in nine bands: eight spectral bands with a resolution of 30 m and one panchromatic band with a resolution of 15 m. The satellite has a temporal resolution of 16 days (Loveland and Irons, 2016). Cloud-free data of December 2019 were acquired from USGS Earth Explorer (<https://earthexplorer.usgs.gov/>) and utilised to calculate the shadow index (SI), bare soil index (BSI), first order (occurrence) texture metric, land surface temperature, and principal component (PC) for this study. Google Earth Engine (GEE) was used to create the annual mean EVI (Enhanced Vegetation Index) and standard deviation of EVI for 2019.

#### 2.2.3. ALOS-2 L band SAR data

JAXA (Japan Aerospace Exploration Agency) launched ALOS-2 with the PALSAR sensor (Phase Array type L-band SAR) in 2014. The PALSAR sensor provides data in three polarimetric modes: single, dual, and quad poles, with a 14-day repetition period. It has three image acquisition modes with varying resolutions: Spotlight mode (1 m \* 3 m), Strip Map mode (10 m), and ScanSAR mode (100 m). This study employed ALOS-2 singlelook complex (SLC) level 1.1 data in strip map mode. The data were obtained via the ALOS-2/ALOS user interface gateway (<https://auig2.jaxa.jp/openam/UI/Login>) as part of the RA6 announcement of opportunity (PI3181). Table 1 lists the ALOS-2 scenes that were used in this study.

**Table 1.** List of ALOS-2 L band SAR, GEDI LiDAR and Landsat-8 OLI scenes used in the study.

#### 2.2.4. Rainfall data

Changes in SAR backscatter from both soil and plants can occur due to rain events. Therefore, a minimum period of five (5) days without rainfall prior to the satellite pass was considered to avoid the effect of rain on SAR backscattered values. Bazzi et al. (2020) and El Hajj et al. (2018) observed that after three days, the likelihood of identifying rainfall events decreases with C-band and X-band SAR. The daily precipitation data from the year 2019, recorded at the carbon flux tower (ISRO-CAP (Climate Atmosphere Programme)) located within TCFD, was utilised to filter the SAR scenes.

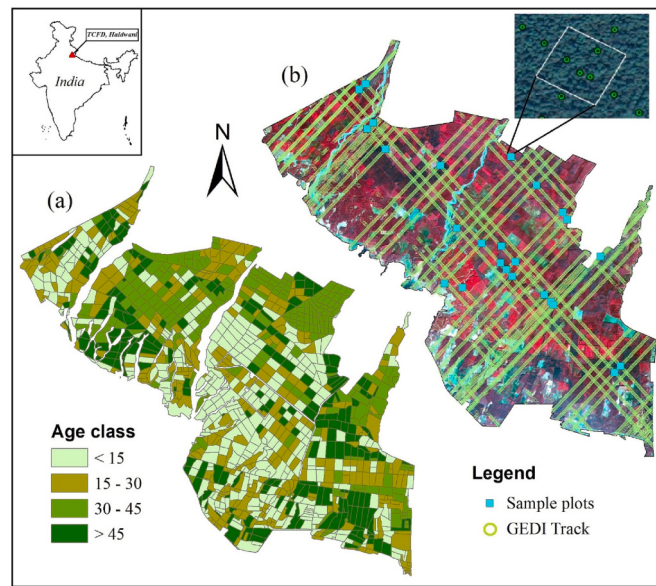


**Fig. 1.** Location of the study area (a) Gradation of forest stand age in the study area (b) GEDI tracks and location of field AGB plots.

**Table 1**  
List of ALOS-2 L band SAR; GEDI LiDAR scenes used in the study.

Sl. No.	ALOS-2 Scene ID	Date	Mode	Incidence angle	Orbit Direction
Advanced Land Observing Satellite (ALOS) 2					
1.	ALOS225456 0570-190,208	19 Feb 2019	Strip	39.7	Ascending
2.	ALOS227319 0570-190,614	14 Jun 2019	Strip	39.7	Ascending
3.	ALOS229389 0570-191,101	01 Nov 2019	Strip	39.7	Ascending
Global Ecosystem Dynamics Investigation LiDAR Product					
1	GEDI02_A & GEDI02_B	2019	Year	Day of year	
2	GEDI02_A & GEDI02_B	2020		117, 121, 124, 128, 149, 167, 185, 193, 200, 255, 294, 305, 316, 331 20, 99, 103, 122, 126, 130, 165, 169, 208, 212, 216, 220, 224, 228, 235, 239	
Landsat 8-OLI					
1	Path: 145 Row: 040	2019		63, 79, 95, 111, 127, 143, 159, 239, 287, 319, 335	

### 2.3. Field inventory and plot AGB estimation

#### 2.3.1. Field sampling design

All GEDI LiDAR tracks that passed through TCFD between April 2019 and August 2020 were downloaded (Fig. 1). In this investigation, only full-power laser beams were considered. Coverage laser beams were filtered out due to their poor sensitivity to canopy height (Duncanson et al., 2022; Hancock et al., 2019). To tackle the geolocation inaccuracies in GEDI footprints, 1-ha field inventory plots were employed in the study. One (1)-ha plots at GEDI tracks crisscrossed the site with a minimum of four (4) GEDI footprints within the plot, were setup and inventoried. Inventory of total 25 sample plots representing plantation type and age class (Fig. 1) was carried out during December and January of 2019.

#### 2.3.2. Inventory and data analysis

The circumference at breast height (CBH) (measured with a tape) and height (measured with a laser rangefinder) of each tree in the plot were recorded. AGB was calculated using species- and site-specific volume equations, wood density (FSI, 1996) and the biomass expansion factor (BEF) (supplementary). The Lorey's height of each plot was calculated by averaging the heights of the dominant and co-dominant tree species in the stand (Lefsky, 2010).

### 2.4. Estimation of canopy height

GEDI provides information on canopy height in term of relative height (RH). The RH are defined as the distance between the elevations of detected ground return and the n% accumulated waveform energy, where n ranges from 1 to 100 (Duncanson et al., 2020). Khati et al. (2021) compared field measured canopy height to RH metrics ranging from RH50 to RH100 and found that the RH95 had the strongest accuracy when compared with field measured canopy height. In this study, RH100, RH98, and RH95 were taken into account and evaluated against field observed canopy height. The best RH was used for retrieval of canopy height.

Spectral and texture information from satellite data has been utilised for forest stand height modelling (Hansen et al., 2013; Hansen et al., 2016). A set of seven remote sensing derived variables were used to estimate canopy height: mean annual EVI, standard deviation of the annual EVI, shadow index (SI), bare soil index (BSI), first order texture metric, principal component (PC3), and land surface temperature (LST). These spectral and textural matrices were obtained from pre-processed Landsat 8 data (Fayad et al., 2016; Freitas et al., 2005; Huete et al., 2002; Rikimaru et al., 2002; Staben et al., 2018). EVI was computed as follows:

$$EVI = 2.5 \times \frac{NIR - RED}{NIR + 6 \times RED - 7.5 \times BLUE + 1}$$

Mean annual EVI and standard deviation were computed for year 2019.

The principal component (PC) highlights the vertical variability of the vegetation (Huete et al., 2002). The PCs of Landsat 8's Blue, Green, Red, NIR, and SWIR bands were calculated, and PC3 was employed for the study. PC3 was used considering the high load factors of Near-infrared (B4) (-0.718) (Karabulut and Küçükönder, 2019) in the PC3 component.

The following equation was used for shadow index (SI) calculation:

$$SI = ((1 - BLUE) \times (1 - GREEN) \times (1 - RED))^{1/3}$$

Bare soil index (BSI) was calculated as:

$$BSI = \frac{(RED + SWIR) - (NIR + BLUE)}{(RED + SWIR) + (NIR + BLUE)}$$

In addition to spectral variables, the first order (occurrence) mean

texture metric was used, which was computed as follows:

$$Mean (M) = \sum_{i=0}^{N_g-1} iP(i)$$

Where  $P(i)$  = probability of each pixel value.

$N_g$  = number of distinct grey levels in the quantized image.

Above-mentioned variables along with RH95 of 150 GEDI footprints were used to predict spatially continuous canopy height of the study area using RF.

### 2.5. AGB estimation through integration of multi-sensor information

#### 2.5.1. Estimation of AGB for GEDI footprints for secondary data generation

It was not feasible to establish several 1-ha sample plots across the entire study area; thus, only representative sample plots (25 plots) were inventoried at the GEDI cross-tracks footprints. However, more sample plots are required for training and validating machine-learning algorithms to predict AGB throughout the study area. Hence, RF regression was used to assess the AGB of the unsampled GEDI footprints using GEDI metrics RH95%, plant area index (PAI), foliage cover, foliage height diversity (FHD), and gap in foliage canopy.

#### 2.5.2. Evaluation of the relationship between SAR backscatter and AGB

Daily precipitation data of 2019 from carbon flux tower in the study area was examined to determine the time with least influence on SAR backscatter from plant and soil moisture. Three scenes of ALOS-2 L dualpol (HH and HV) SAR for the months of February, June, and November were acquired. The Sentinel Application Platform software (SNAP) was used for pre-processing of ALOS-2 scenes and generation of the sigma-naught images. The sigma-naught values of HH and HV polarisation for various months were regressed against the field measured AGB, and the month with maximum  $R^2$  value was considered best for estimation of AGB in the study area.

#### 2.5.3. AGB estimation using random Forest algorithm

The spatial AGB of the study area was predicted using two approaches. In the first approach, the AGB was calculated using only the variables generated from the ALOS-2 SAR. While in the second approach, canopy height was included as an additional parameter in RF along with the SAR variables to estimate AGB. Finally, the best spatial AGB estimate was determined by comparing the  $R^2$  and RMSE of the model predicted AGB.

#### 2.5.4. Estimation of uncertainty in predicted AGB models

To evaluate the uncertainty in the spatial AGB prediction, the standard deviation per pixel of the RF model was calculated by running the RF model numerous times on a subset of the AGB data from the field plots (training data). Fig. 2 depicts the flowchart of the overall methodology.

## 3. Results

### 3.1. Spatial estimation of canopy height

The relationship between field measured canopy height and GEDI RH100, RH98, and RH95 is shown in Fig. 3. The canopy height and RH95 had the best correlation (adjusted  $R^2 = 0.70$ ). Compared to mixed stands, pure stands provided a better estimate of canopy height from RH95. In the RF model, the spatial canopy height was predicted using 150 numbers of GEDI RH95 footprints as the dependent variable and seven Landsat-8 variables as the independent variables. The RF model with  $Ntree = 500$  and  $Mtry = 3$  achieved the lowest out-of-bag error at around 100 Ntree. In the study area, the top predictor variables of canopy height were BSI, mean EVI, mean texture, and shade index (Fig. 4a). With  $R^2 = 0.97$  and RMSE = 2.32 m, the RF performance in

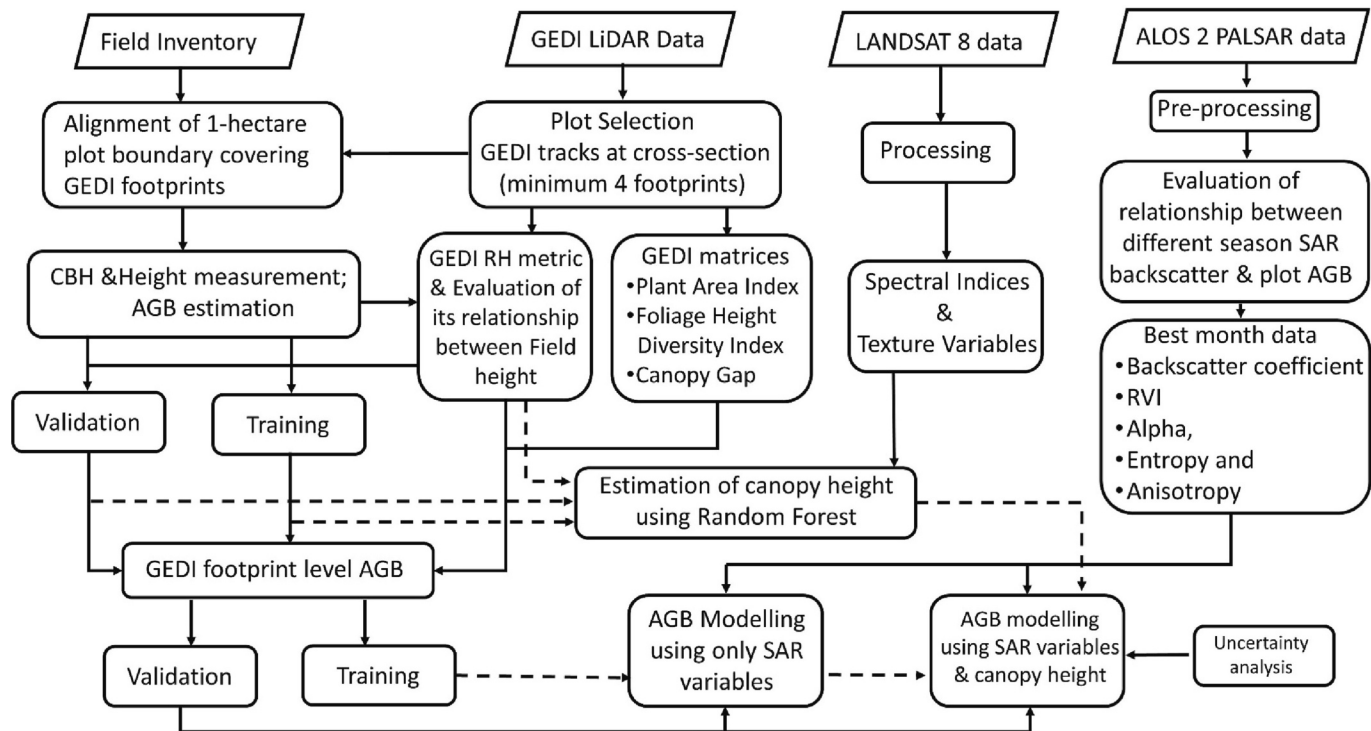


**Fig. 2.** Flowchart of the overall methodology for estimating AGB using Landsat-OLI, ALOS-2 L-band SAR, and GEDI metrics.

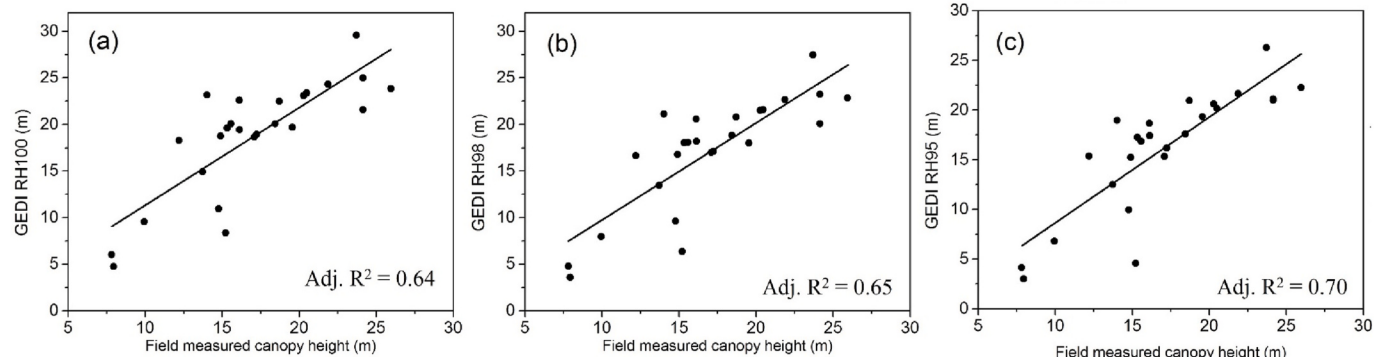


**Fig. 3.** Relationship between field measured canopy height and GEDI canopy height at (a) RH100, (b) RH98, and (c) RH95.

predicting canopy height was very precise. In the study area, predicted canopy heights ranged from 20 to 30 m for teak, 10–20 m for Eucalyptus, 10–15 m for Poplar, and 10–25 m for mixed species stands.

### 3.2. Prediction of AGB at GEDI footprints

Pure stands of Eucalyptus (adjusted  $R^2 = 0.47$ ) and Teak (adj.  $R^2 = 0.42$ ) had a stronger relationship between canopy height and AGB than mixed stands (adj.  $R^2 = 0.17$ ). In the study area, GEDI canopy height (RH95) has a curvilinear relationship with AGB (adj.  $R^2 = 0.64$ ). Plot-specific information on field measured canopy height and AGB are provided in supplementary information. The relationship between canopy height and AGB was curvilinear, with an adjusted  $R^2$  of 0.57. The predicted AGB ranged from 23.93 to 198.55 Mg ha<sup>-1</sup> (Fig. 5). The estimated AGB at the GEDI footprint had an  $R^2$  of 0.91 and an RMSE of 20.10 Mg ha<sup>-1</sup>. FHD was the most important predictor variable in the model, followed by canopy gap percentage.

### 3.3. AGB prediction using SAR variables

The logarithmic fit best described the relationship between ALOS-2 L band SAR HH & HV backscatter and field estimated AGB in early winter (November), late winter (February), and late summer (June) (Fig. 6). HV polarisation demonstrated moderate sensitivity to AGB in February and November, with adjusted  $R^2$  values of 0.33 and 0.31, respectively. The strongest relationship between AGB and SAR backscatter was observed with HV polarisation of June month, with an adjusted  $R^2$  of 0.51. In February and November, the sensitivity of SAR backscatter to AGB in HH polarisation was lower, with adj.  $R^2$  values of 0.16 and 0.23, respectively. In June, there was a higher sensitivity to AGB, with an adj.  $R^2$  of 0.46. The saturation of the L-band SAR backscatter was more noticeable in the HH polarisation (approximately at 150 Mg ha<sup>-1</sup>) than in the HV polarisation.

The SAR data from June month was chosen for RF-based AGB prediction because it had the highest  $R^2$  between SAR backscatter and AGB. The least OOB error was observed in the RF model generated solely from SAR variables at around 65 Ntree. In the AGB model, the strongest predictor variables were discovered to be HV, RVI, and HH (Fig. 7a). The

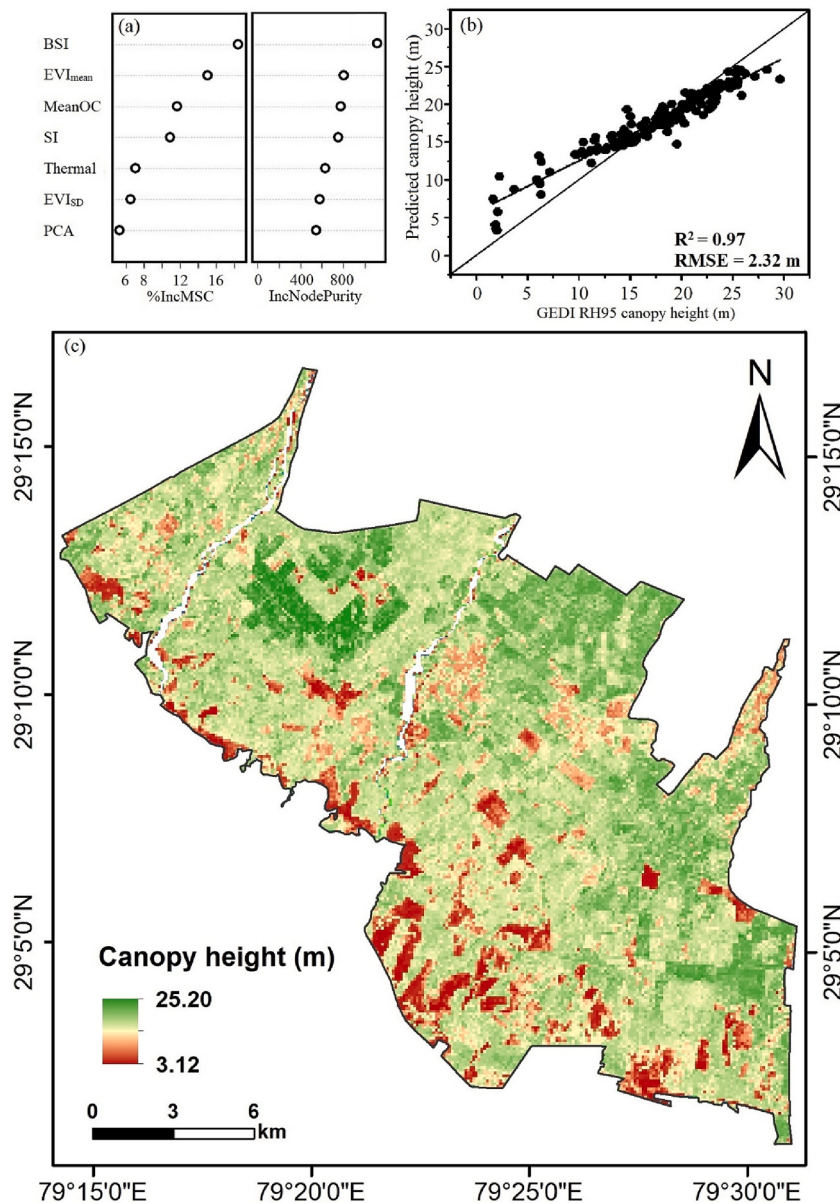


**Fig. 4.** Estimation of spatial canopy height (a) Important predictors variables, (b) model validation, and (c) spatial canopy height of the study area.

AGB was predicted with an  $R^2$  of 0.61 and an RMSE of  $18.27 \text{ Mg ha}^{-1}$ . Alpha, entropy, and anisotropy all played minor roles in predicting AGB. Uncertainty estimates for the AGB model ranged from  $0.64 \text{ Mg ha}^{-1}$  to  $28.66 \text{ Mg ha}^{-1}$ . It was found that SAR-based RF model prediction underestimates for high AGB of taller plantation stands.

#### 3.4. AGB prediction using canopy height and SAR variables

The spatial canopy height was included in this step along with the SAR variables in the RF model. In the RF model, canopy height surpass HV, HH, and RVI as the most significant predictors of AGB. With an AGB prediction  $R^2$  of 0.77 and an RMSE of  $13.86 \text{ Mg ha}^{-1}$  (Fig. 8), the model performance was observed to be superior than AGB model based solely on SAR-variables. Alpha, entropy, and anisotropy—all polarimetric variables—had less of an impact on AGB prediction. The AGB map (Fig. 8c) reveals that incorporating spatial canopy height into the SAR-based RF model improves prediction of spatial AGB variability across the study area, providing a better estimate of AGB for taller stands and a modest improvement in AGB range. The AGB uncertainty map shows that the highest uncertainty was in low biomass areas corresponding to

young plantations.

#### 4. Discussion

The GEDI information metrics offer enormous potential to assess vertical vegetation structure at the landscape level. However, the performance of GEDI must be examined across diverse forest types, density, regions, and variables that affect GEDI performance (Lang et al., 2022). As more global forest height product become accessible, more validation activities are required to examine the appropriateness of canopy height products to forestry demands and to assist the effectiveness of the next generation global height products (Pascual et al., 2022). GEDI RHs are sensitive to ground-finding accuracy, and the performance of RHs estimates varies for forest profiles of different forest types (Wang et al., 2022). Various RH values has been employed in studies to determine canopy height (Adam et al., 2020). However, higher percentile metrics (e.g., RH99 or RH100) are frequently influenced by noise, whereas lower percentile metrics (e.g., RH50) are influenced by distorted waveforms or lower-density point clouds (Dhargay et al., 2022). GEDI measured canopy height, when matched with field-measured canopy

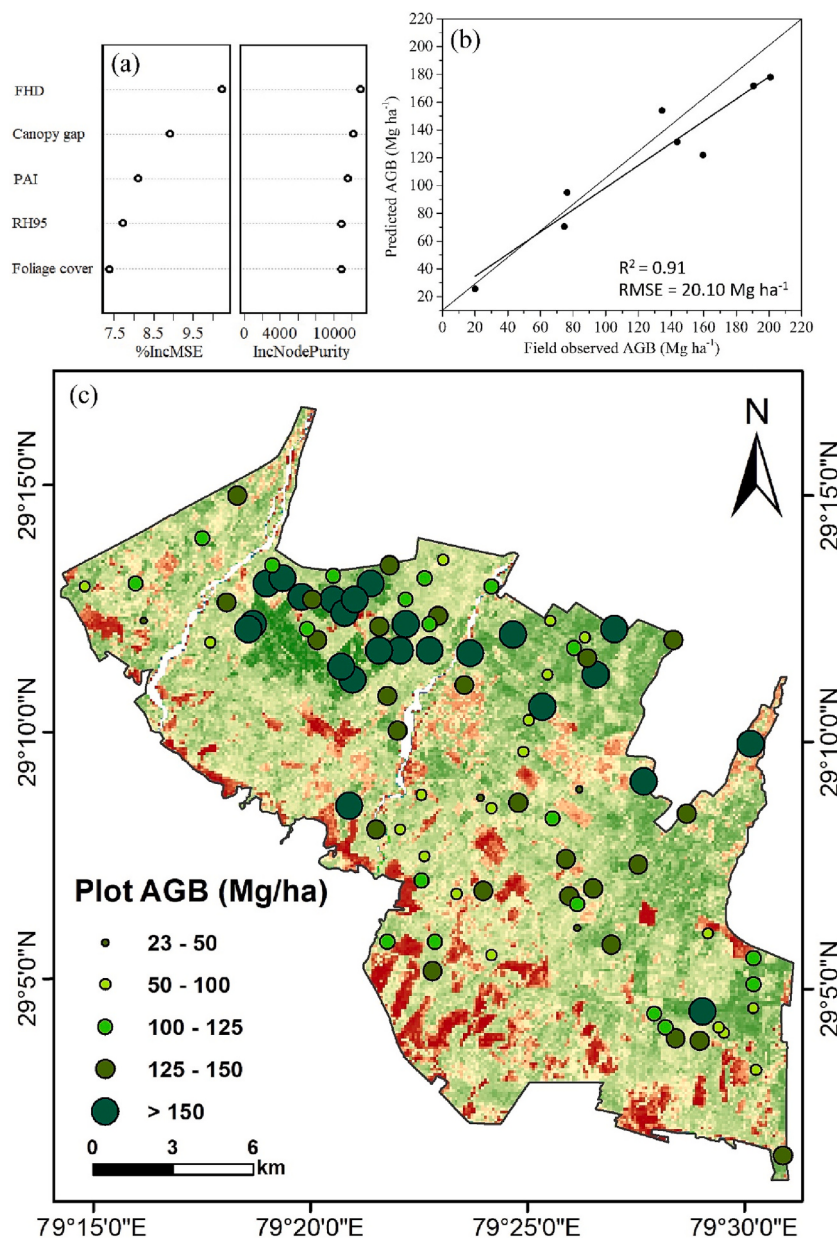


**Fig. 5.** AGB prediction at the GEDI footprints (a) Important predictor variables, (b) model validation, and (c) predicted AGB at GEDI footprints.

height, RH95 provided the best results, followed by RH98 and RH100. Previous research has also reported a strong agreement between field-measured canopy height and GEDI RH95 canopy height (Potapov et al., 2021; Wang et al., 2022). In well-stocked blocks, there was more agreement between the GEDI canopy height and the field-measured canopy height than in open forests with variable tree heights.

A commonly used approach for achieving wall-to-wall canopy height mapping is to combine field-measured canopy heights with optical and/or microwave remote sensing data (Lang et al., 2021; Liang et al., 2023; Potapov et al., 2021). Linear regression, RF, ANN, and machine learning techniques are often utilised to create canopy height prediction models using remote sensing data (Faguna et al., 2019). Using RF algorithm with potential variables (BSI, mean EVI, mean texture, shade index), spatial canopy height was predicted with high accuracy ( $R^2 = 0.97$  and RMSE = 2.32 m). Previous research has demonstrated that EVI, BSI, and crown shadow (Rikimaru et al., 2002) are good predictor of forest structures (Elhag et al., 2021). A global canopy height map at 30 m resolution was generated by extrapolating GEDI canopy height using Landsat data through RF (Potapov et al., 2021). Gupta and Sharma (2022) used

machine-learning algorithm to generate forest spatial height map by integrating multi-spectral optical and SAR data with sparse GEDI footprints data. Similarly, Healey et al. (2020) developed locally calibrated Landsat-based models to extrapolate canopy height from GEDI's samples points.

The spatial discrepancy between the GEDI LiDAR footprints and the inventory plots is expected when integrating the field plots to the GEDI LiDAR footprints. Luthcke et al. (2019) reported a geolocation accuracy of 10 m for GEDI Levels 2A and 2B products of April 2019 to August 2020. Further, the waveform data contains information about the whole forest canopy, making geolocation matching more challenging. According to Roy et al. (2021), geolocation uncertainty in GEDI accounts for 50% of the variation in canopy height estimation, with higher variation in spatially heterogeneous canopies, such as canopies with small forest stands, canopy gaps, and forest edges. Thus, raising concerns on the use of GEDI data acquired over heterogeneous forests and forest edges. Increasing the sample plot size, could potentially improve the representativeness of the GEDI LiDAR canopy height while decreasing the effect of geolocation uncertainty. Given the GEDI tracks

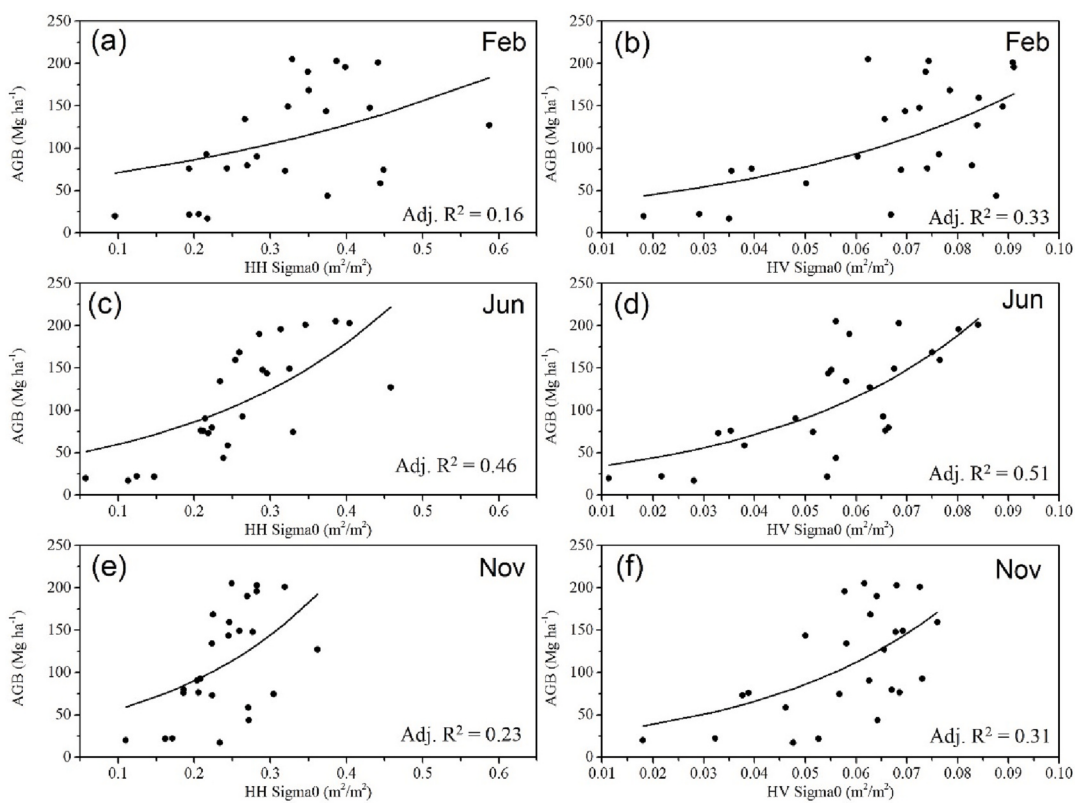


**Fig. 6.** Relationship between ALOS-2 L band HH and HV linear backscatter intensity and AGB.

over the research area were oriented northeast to southwest and northwest to southeast, four power beam footprints were available at the cross-sections, so 1-ha sample plots were setup at GEDI track cross-sections for this study.

Field inventory of a large number of 1-ha sample plots for AGB estimate is a time-consuming and expensive process. However, greater numbers of reference plots are required to represent the AGB range that exists in the area of interest for the calibration and validation of the spatial biomass model. To generate additional AGB sample points, AGB at GEDI footprint was established using the GEDI metrics (PAI, foliage cover, FHD, and gap in foliage canopy). GEDI footprint AGB was predicted with good precision ( $R^2$  of 0.91 and RMSE of  $20.10 \text{ Mg ha}^{-1}$ ). To train and evaluate the forest AGB retrieval model, Khati et al. (2021) produced 2200 AGB sample points at GEDI footprints with an RMSE of  $32 \text{ Mg ha}^{-1}$  using just GEDI canopy height. The use of additional criteria such as PAI, foliage cover, FHD, and the gap in foliage canopy during this study might have contributed to the improvement in RMSE ( $20.10 \text{ Mg ha}^{-1}$ ) in the current study.

Forest AGB has been estimated successfully using L-band SAR data (Cartus et al., 2012; Santoro et al., 2015; Santoro and Cartus, 2018; Tanase et al., 2014; Thiel and Schmullius, 2016) through empirical (Kasischke et al., 1997; Lucas et al., 2006; Watanabe et al., 2006), semi-empirical (Kurvanen et al., 1999), numerical (Burges et al., 2011; Lucas et al., 2004) and machine learning algorithms (Santi et al., 2015; Vafaei et al., 2018). Depending on the season, the sensitivity of the L-band to AGB ranged from  $120$  to  $170 \text{ Mg ha}^{-1}$  (Mitchard et al., 2009; Yu and Saatchi, 2016). In non-homogeneous environmental settings, these fluctuations contribute up to a 300% error in AGB estimations (Bouvet et al., 2018). Over Indian forests, L-band saturates at  $140$ – $160 \text{ Mg ha}^{-1}$  AGB range, and currently available microwave wavelengths alone is not sufficient to predict entire range of biomass (Fararoda et al., 2021).

The season in which SAR data is collected is critical for satellite-based estimations of AGB (Nguyen et al., 2020). The best relationship between AGB and SAR backscatter was observed in June during the

study period, which is expected given that the forest in the study area experiences peak dry conditions in June. The dry season in the study region begins in the last week of February and lasts until the first week of July. Rainfall data analysis revealed that merely  $125.47 \text{ mm}$  of the total  $995.44 \text{ mm}$  in 2019 occurred between January to June. Dry season SAR data is more significant than rainy season data for determining biomass (Nguyen et al., 2020). The link between SAR backscatter and AGB is influenced by soil and canopy moisture, seasonal variations in canopy structure, and weather (Lucas et al., 2010; Pulliainen et al., 1999; Rauste, 2005). The form of the relationship and the asymptotes or saturation values between SAR backscatter and AGB vary greatly depending on environmental conditions and changes in soil moisture (Saatchi, 2019). Thus, selecting the optimal season to maximize the relationship between AGB and SAR information has the potential to improve AGB estimates when using SAR data.

RF model based solely on the SAR variables, had an  $R^2$  of 0.61 and an RMSE of  $18.27 \text{ Mg ha}^{-1}$  during the research. Khati et al. (2021) estimated AGB with  $R^2$  of 0.78 and RMSE of  $27.1 \text{ Mg ha}^{-1}$  using a multi-temporal L-band ALOS-2 and the three-parameter water cloud model. Thumayat et al. (2016) estimated the AGB of central Indian deciduous forests with RMSE of  $19.32 \text{ Mg ha}^{-1}$  and  $R^2$  of 0.70 utilising the empirical relationship between SAR HV backscatter and AGB. Studies have established a strong relationship between AGB and LiDAR height metrics; however, these relationships are site-specific (Ni-Meister et al., 2022). Dorado-Roda et al. (2021) found GEDI metrics to be potentially useful for improving the AGB models.

Improvement in AGB estimation with better  $R^2$  of 0.77 and RMSE of  $13.86 \text{ Mg ha}^{-1}$  was observed during the study when canopy height information was incorporated along with the L-band SAR variables in the RF model. The addition of height data reduced the model RMSE by  $4.41 \text{ Mg ha}^{-1}$  and predicted a wider range of AGB, which coincides with taller and denser forest stands. The forest vertical characteristics are significantly related to the AGB, and they are not affected by data saturation (Wang et al., 2018). Forest canopy height represents the vertical

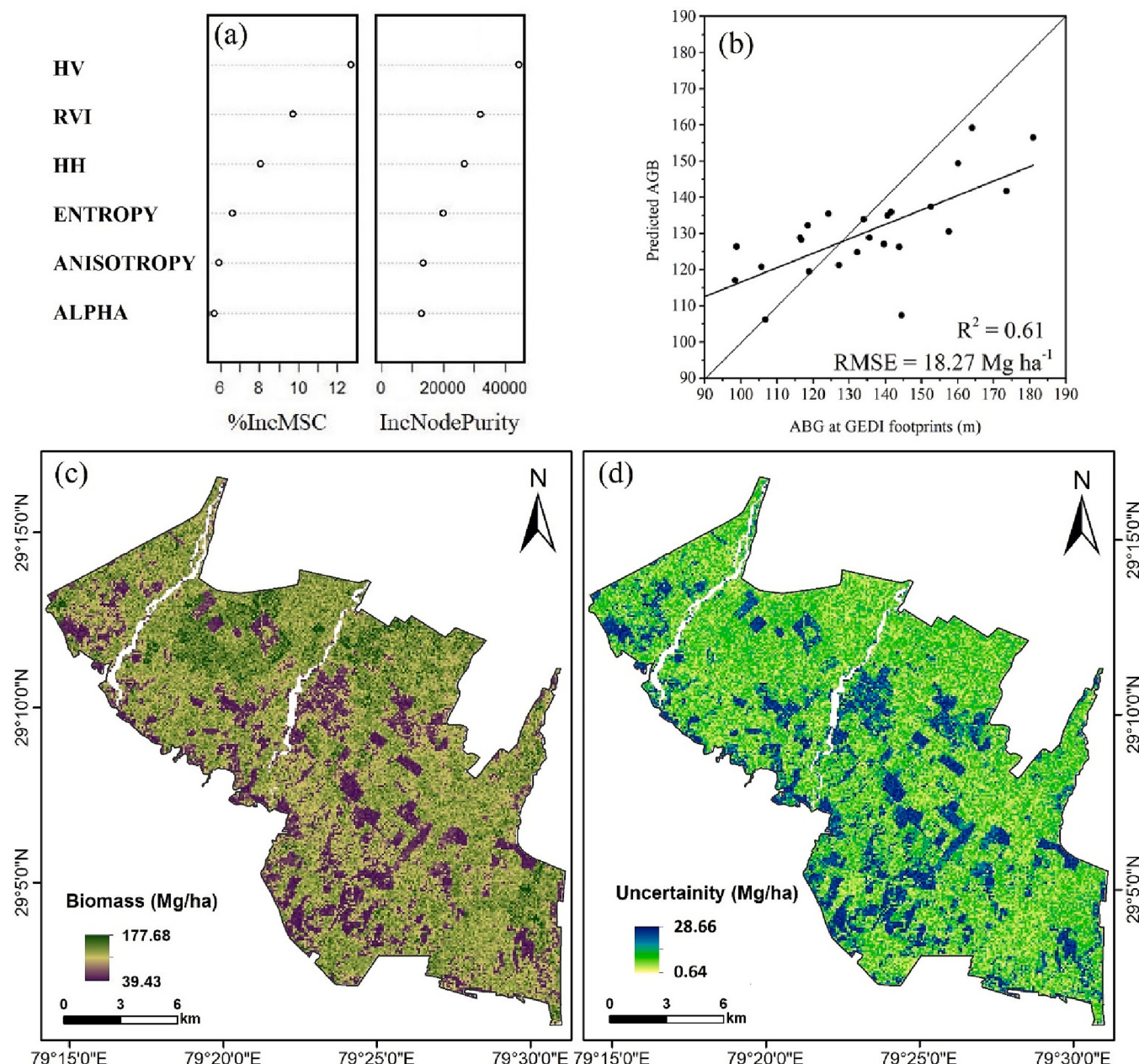


**Fig. 7.** AGB modelling with SAR variables (a) important predictor variables, (b) validation of AGB model (c) spatial AGB map, and (d) AGB uncertainty map of the study area.

structure characteristic, which is different from the information provided by spectral features and can alleviate the biomass saturation problem in AGB estimations. The accuracy of AGB estimation for individual trees and subsequently for plot AGB fundamentally depends on the accuracy of tree height measurements (Hunter et al., 2013). Santoro (2003) reported a reasonably good correlation between tree heights and tree volumes, with a coefficient of determination of 0.89. In place of using allometric functions, a straightforward regression equation based on tree height measurements can be used to estimate tree volume and vice versa (Askne et al., 1997; Santoro et al., 1999; Santoro et al., 2002). Chen et al. (2021) overcome the issue of saturation by integrating GEDI LiDAR, Sentinel-1 SAR, Sentinel-2 Multispectral Instrument (MSI), and ALOS DSM data during AGB estimation of a mountain mixed forests. Yadav et al. (2021) used TanDEM-X pair-derived canopy height and 11 optimal parameters (e.g. Alpha angle, coherence, etc.) predicted AGB with  $R^2$  of 0.83 and RMSE of 27  $Mg\ ha^{-1}$ .

The uncertainty was in the range of 0.98 to 26.70  $Mg\ ha^{-1}$ , the overall uncertainty was less than 20%. Higher uncertainties were observed in the younger plantation (less than 5 years). Three plausible reasons for the higher uncertainty could be (i) a lower number of samples, (ii) lower interaction of L-band SAR with sparse vegetation, and (iii) an overestimation of canopy heights by GEDI.

Dorado-Roda et al. (2021) found that GEDI canopy height retrieval performed better in denser and homogeneous coniferous forests than in sparse forests, demonstrating the impact of forest structure on GEDI canopy height retrieval. Dang et al. (2019) reported an average uncertainty value of 31.99  $Mg\ ha^{-1}$  within a range of 9.87 to 93.27  $Mg\ ha^{-1}$ , with higher uncertainty values in sparse vegetative areas than in dense forest areas. Likewise, increased uncertainty was observed in seasonal grassland, scrubs, and along the fringes during the AGB estimation of a mangrove forests (Prakash et al., 2022). Field plot AGB estimations are also subjected to certain uncertainty due to allometric factors, wood

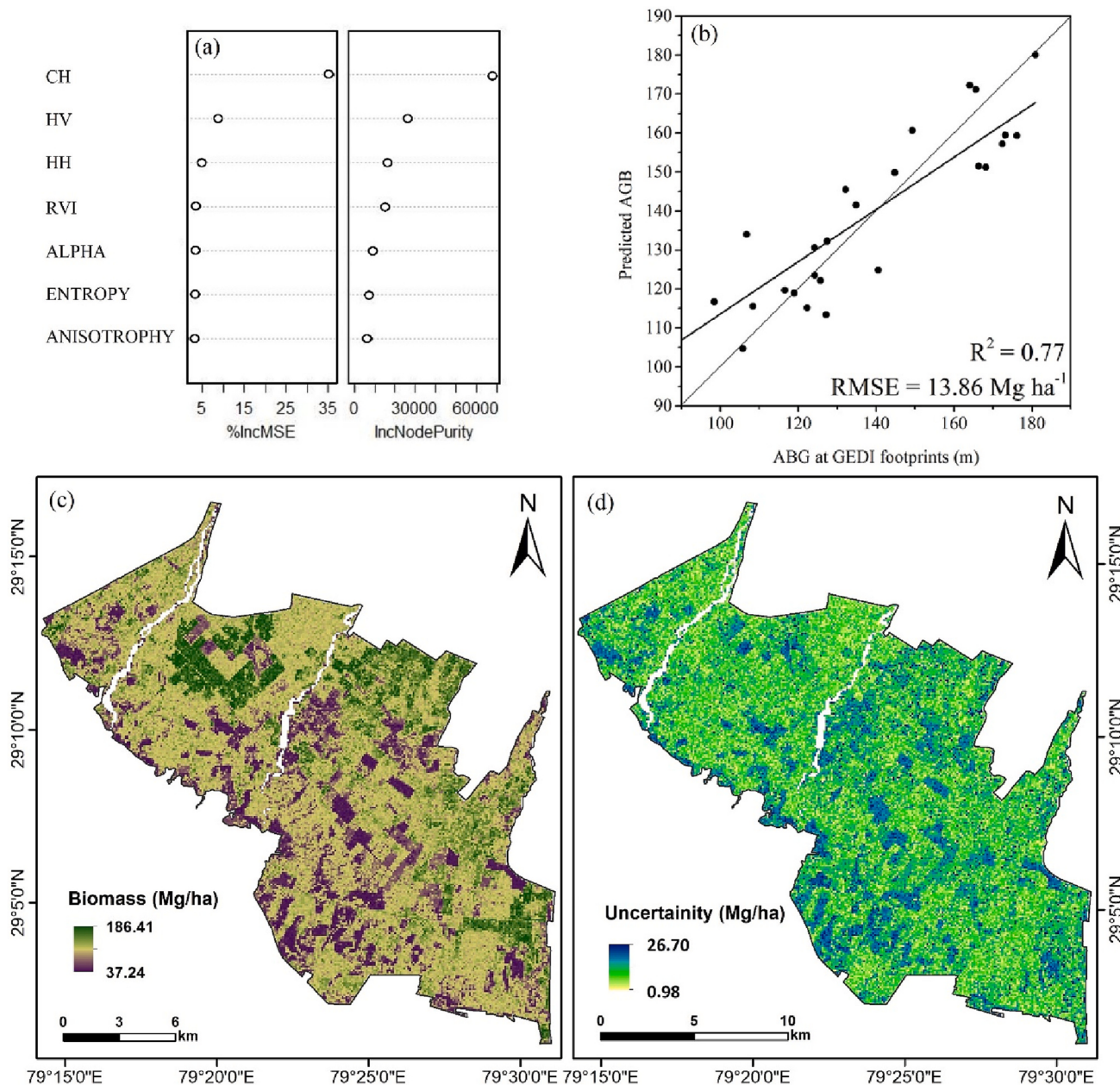


**Fig. 8.** AGB modelling with canopy height and SAR variables (a) important predictor variables, (b) validation of AGB model (c) spatial AGB map, and (d) AGB uncertainty map of the study area.

density, and observation error (Chave et al., 2004). In tropical forests, 5% (5%) errors in 1-ha field plot is due to allometric equations (Chave et al., 2004). Incorporating historical data, such as regional variability, could help quantify the uncertainty associated with forest AGB estimation (Do et al., 2022). Difficulties associated with measuring AGB using field measurement standards, could contribute high uncertainty in the quantity and spatial distribution of AGB (Lefsky, 2010; Simard et al., 2011). Field campaigns, ideally combined with destructive tree harvesting to reduce uncertainties in allometries, and airborne LiDAR, would be particularly useful to improve our understanding of the AGB (Mitchard et al., 2013). The applicability of our approach can be expanded by testing its performance with L-band SAR and GEDI data for various bioclimatic regions, topographies, and growth stages. Lastly, AGB allometry for young growth/planting is required to improve AGB estimation and modelling.

## 5. Conclusion

With the availability of space-based GEDI-LiDAR data in the public domain, there is increasing interest in use of canopy height information for improved AGB estimation. Generally, managed forest for production forestry has a high variable in stand height, which can be effectively captured through LiDAR remote sensing. Thus, facilitate precise estimation of AGB for better management of forest resources. Our study demonstrates the synergistic use of Landsat-8, ALOS-2 L-band and GEDI data for improving AGB estimation. One-hectare (ha) sample plot design was adopted in order to improve the integration of GEDI footprints with in-situ, optical, and SAR data. GEDI metrics information viz., RH95, PAI, foliage cover, FHD and gap in foliage canopy are strong proxy ( $R^2 = 0.91$ ) of AGB and thus can be used for generation of secondary AGB plot data at the GEDI footprint level for calibration and validation of spatial biomass models at larger scale. Landsat-8 derived variables (EVI, BSI and crown shade) with sparse GEDI data can assist in generation of

continuous spatial canopy height information for improving AGB models. The study found that incorporating canopy height information along with L-band SAR derived variables in the AGB model not only improves the accuracy of the AGB estimate but also reduces the issue of saturation often observed with SAR or optical data when used alone. Thus, the study concludes that optical, SAR and LiDAR can be effectively integrated for precise AGB estimation of managed tropical forest with highly variable stand height. The present study is limited by restricted availability of spaceborne LiDAR data/footprints and L-band SAR data. With upcoming new satellite missions (NISAR and EarthCARE), refinement and adoption of the methodology for improved and large-scale forest AGB mapping is possible.

## Declaration of Competing Interest

The authors declare that they have no known competing financial interests or personal relationships that could have appeared to influence the work reported in this paper.

## Data availability

Data will be made available on request.

## Acknowledgments

The authors are thankful to JAXA for providing ALOS-2 PALSAR data as part of the RA6 Announcement of Opportunity (PI3181), the Landsat science team, GEDI Science team for making data available to the user community. The authors sincerely thank the Director, Indian Institute of Remote Sensing, ISRO, Dehradun, for the encouragement and support for this study. The author thanks the Soil-Vegetation- Atmosphere-Flux (SVAF)-Climate Atmospheric Programme, ISRO for sharing the rainfall data. Thanks are also due to the anonymous reviewers for their valuable suggestions, which helped us to improve the manuscript.

## Appendix A. Supplementary data

Supplementary data to this article can be found online at <https://doi.org/10.1016/j.ecoinf.2023.102234>.

## References

- Adam, M., Urbazaev, M., Dubois, C., Schmullius, C., 2020. Accuracy assessment of GEDI terrain elevation and canopy height estimates in European temperate forests: influence of environmental and acquisition parameters. *Remote Sens.* 12, 3948. <https://doi.org/10.3390/rs12233948>.
- Ahmed, R., Siqueira, P., Hensley, S., Chapman, B., Bergen, K., 2011. A survey of temporal decorrelation from spaceborne L-band repeat-pass InSAR. *Remote Sens. Environ.* 115, 2887–2896. <https://doi.org/10.1016/j.rse.2010.03.017>.
- Askne, J.I.H., Dämmert, P.B.G., Ulander, L.M.H., Smith, G., 1997. C-band repeat-pass interferometric SAR observations of the forest. *IEEE Trans. Geosci. Remote Sens.* 35, 25–35. <https://doi.org/10.1109/36.551931>.
- Asner, G.P., Clark, J.K., Mascaro, J., Galindo García, G.A., Chadwick, K.D., Navarrete Encinales, D.A., Paez-Acosta, G., Cabrera Montenegro, E., Kennedy-Bowdoin, T., Duque, Á., Balaji, A., von Hildebrand, P., Maatoug, L., Phillips Bernal, J.F., Yepes Quintero, A.P., Knapp, D.E., García Dávila, M.C., Jacobson, J., Ordóñez, M.F., 2012. High-resolution mapping of forest carbon stocks in the Colombian Amazon. *Biogeosciences* 9, 2683–2696. <https://doi.org/10.5194/bg-9-2683-2012>.
- Baccini, A., Goetz, S.J., Walker, W.S., Laporte, N.T., Sun, M., Sulla-Menashe, D., Hackler, J., Beck, P.S.A., Dubayah, R., Friedl, M.A., Samanta, S., Houghton, R.A., 2012. Estimated carbon dioxide emissions from tropical deforestation improved by carbon-density maps. *Nat. Clim. Chang.* 2, 182–185. <https://doi.org/10.1038/nclimate1354>.
- Balzter, H., 2001. Forest mapping and monitoring with interferometric synthetic aperture radar (InSAR). *Prog. Phys. Geogr.* 25, 159–177. <https://doi.org/10.1177/03091330102500201>.
- Balzter, H., Rowland, C.S., Saich, P., 2007. Forest canopy height and carbon estimation at monks wood National Nature Reserve, UK, using dual-wavelength SAR interferometry. *Remote Sens. Environ.* 108, 224–239. <https://doi.org/10.1016/j.rse.2006.11.014>.
- Bazzi, H., Baghdadi, N., Fayad, I., Charron, F., Zribi, M., Belhouchette, H., 2020. Irrigation events detection over intensively irrigated grassland plots using Sentinel-1 data. *Remote Sens.* 12, 4058. <https://doi.org/10.3390/rs12244058>.
- Boisvenue, C., Smiley, B.P., White, J.C., Kurz, W.A., Wulder, M.A., 2016. Integration of Landsat time series and field plots for forest productivity estimates in decision support models. *For. Ecol. Manag.* 376, 284–297. <https://doi.org/10.1016/j.foreco.2016.06.022>.
- Bouvet, A., Mermoz, S., le Toan, T., Villard, L., Mathieu, R., Naidoo, L., Asner, G.P., 2018. An above-ground biomass map of African savannas and woodlands at 25 m resolution derived from ALOS PALSAR. *Remote Sens. Environ.* 206, 156–173. <https://doi.org/10.1016/j.rse.2017.12.030>.
- Burgin, M., Clewley, D., Lucas, R.M., Moghaddam, M., 2011. A generalized radar backscattering model based on wave theory for multilayer multispecies vegetation. *IEEE Trans. Geosci. Remote Sens.* 49 (12), 4832–4845. <https://doi.org/10.1109/TGRS.2011.2172949>.
- Cartus, O., Santoro, M., Kellndorfer, J., 2012. Mapping forest aboveground biomass in the northeastern United States with ALOS PALSAR dual-polarization L-band. *Remote Sens. Environ.* 124, 466–478. <https://doi.org/10.1016/j.rse.2012.05.029>.
- Chave, J., Condit, R., Aguilar, S., Hernandez, A., Lao, S., Perez, R., 2004. Error propagation and scaling for tropical forest biomass estimates. *Philos. Trans. R. Soc. Lond. Ser. B Biol. Sci.* 359, 409–420. <https://doi.org/10.1098/rstb.2003.1425>.
- Chen, L., Ren, C., Zhang, B., Wang, Z., Liu, M., Man, W., Liu, J., 2021. Improved estimation of forest stand volume by the integration of GEDI LiDAR data and multi-sensor imagery in the Changbai Mountains mixed forests ecoregion (CMMFE), Northeast China. *Int. J. Appl. Earth Obs. Geoinf.* 100, 102326. <https://doi.org/10.1016/j.jag.2021.102326>.
- Chen, Q., Vaglio Laurin, G., Battles, J.J., Saah, D., 2012. Integration of airborne lidar and vegetation types derived from aerial photography for mapping aboveground live biomass. *Remote Sens. Environ.* 121, 108–117. <https://doi.org/10.1016/j.rse.2012.01.021>.
- Chi, H., Sun, G., Huang, J., Guo, Z., Ni, W., Fu, A., 2015. National forest aboveground biomass mapping from ICESat/GLAS data and MODIS imagery in China. *Remote Sens.* 7, 5534–5564. <https://doi.org/10.3390/rs70505534>.
- Chrysafis, I., Mallinis, G., Tsakiri, M., Patias, P., 2019. Evaluation of single-date and multi-seasonal spatial and spectral information of Sentinel-2 imagery to assess growing stock volume of a Mediterranean forest. *Int. J. Appl. Earth Obs. Geoinf.* 77, 1–14. <https://doi.org/10.1016/j.jag.2018.12.004>.
- Dang, A.T.N., Nandy, S., Srinet, R., Luong, N.V., Ghosh, S., Senthil Kumar, A., 2019. Forest aboveground biomass estimation using machine learning regression algorithm in Yok Don National Park, Vietnam. *Ecol. Inform.* 50, 24–32. <https://doi.org/10.1016/j.ecoinf.2018.12.010>.
- Dhanda, P., Nandy, S., Kushwaha, S.P.S., Ghosh, S., Murthy, Y.K., Dadhwali, V.K., 2017. Optimizing spaceborne LiDAR and very high resolution optical sensor parameters for biomass estimation at ICESat/GLAS footprint level using regression algorithms. *Prog. Phys. Geogr.* 41, 247–267. <https://doi.org/10.1177/030913317693443>.
- Dhargay, S., Lyell, C.S., Brown, T.P., Inbar, A., Sheridan, G.J., Lane, P.N.J., 2022. Performance of GEDI space-borne LiDAR for quantifying structural variation in the temperate forests of south-eastern Australia. *Remote Sens.* 14 (15), 3615. <https://doi.org/10.3390/rs14153615>.
- Do, A.N.T., Tran, H.D., Ashley, M., Nguyen, A.T., 2022. Monitoring landscape fragmentation and aboveground biomass estimation in can Gio mangrove biosphere reserve over the past 20 years. *Ecol. Inform.* 70, 101743. <https://doi.org/10.1016/j.ecoinf.2022.101743>.
- Dorado-Roda, I., Pascual, A., Godinho, S., Silva, C.A., Botequim, B., Rodríguez-Gonzálvez, P., González-Ferreiro, E., Guerra-Hernández, J., 2021. Assessing the accuracy of gedi data for canopy height and aboveground biomass estimates in mediterranean forests. *Remote Sens.* 13, 2279. <https://doi.org/10.3390/rs13122279>.
- Dubaya, S.T., 2021. Global Ecosystem Dynamics Investigation (GEDI) Level 2 User Guide College Park, University of Maryland, MD.
- Dubayah, R., Blair, J.B., Goetz, S., Fatoyinbo, L., Hansen, M., Healey, S., Hofton, M., Hurnt, G., Kellner, J., Luthcke, S., Armston, J., Tang, H., Duncanson, L., Hancock, S., Jantz, P., Marselis, S., Patterson, P.L., Qi, W., Silva, C., 2020. The global ecosystem dynamics investigation: high-resolution laser ranging of the Earth's forests and topography. *Sci. Remote Sens.* 1, 100002. <https://doi.org/10.1016/j.srs.2020.100002>.
- Dubayah, R.O., Armston, J., Healey, S.P., Yang, Z., Patterson, P.L., Saarela, S., Stahl, G., Duncanson, L., Kellner, J.R., 2022. GEDI L4B Gridded Aboveground Biomass Density, Version 2. ORNL DAAC, Oak Ridge, Tennessee, USA. <https://doi.org/10.3334/ORNLDAAC/2017>.
- Dubovik, O., Schuster, G.L., Xu, F., Hu, Y., Bösch, H., Landgraf, J., Li, Z., 2021. Grand challenges in satellite remote sensing. *Front. Remote Sens.* 2, 619818. <https://doi.org/10.3389/fresn.2021.619818>.
- Duncanson, L., Neuenschwander, A., Hancock, S., Thomas, N., Fatoyinbo, T., Simard, M., Silva, C.A., Armston, J., Luthcke, S.B., Hofton, M., Kellner, J.R., Dubayah, R., 2020. Biomass estimation from simulated GEDI, ICESat-2 and NISAR across environmental gradients in Sonoma County, California. *Remote Sens. Environ.* 242, 111779. <https://doi.org/10.1016/j.rse.2020.111779>.
- Duncanson, L., Kellner, J.R., Armston, J., Dubayah, R., Minor, D.M., Hancock, S., Healey, S.P., Patterson, P.L., Saarela, S., Marselis, S., Silva, C.E., Bruening, J., Goetz, S.J., Tang, H., Hofton, M., Blair, B., Luthcke, S., Fatoyinbo, L., Abernethy, K., Alonso, A., Zgraggen, C., 2022. Aboveground biomass density models for NASA's global ecosystem dynamics investigation (GEDI) lidar mission. *Remote Sens. Environ.* 270, 112845. <https://doi.org/10.1016/j.rse.2021.112845>.
- El Hajj, M., Baghdadi, N., Bazzi, H., Zribi, M., 2018. Penetration analysis of SAR signals in the C and L bands for wheat, maize, and grasslands. *Remote Sens.* 11, 31. <https://doi.org/10.3390/rs11010031>.

- Elhag, M., Boteva, S., Al-Amri, N., 2021. Forest cover assessment using remote-sensing techniques in Crete Island, Greece. *Open Geosci.* 13, 345–358. <https://doi.org/10.1515/geo-2020-0235>.
- Fagua, J.C., Jantz, P., Rodriguez-Buriticá, S., Duncanson, L., Goetz, S.J., 2019. Integrating LiDAR, multispectral and SAR data to estimate and map canopy height in tropical forests. *Remote Sens.* 11, 2697. <https://doi.org/10.3390/rs11222697>.
- Fararoda, R., Reddy, R.S., Rajashekhar, G., Chand, T.K., Jha, C.S., Dadhwal, V.K., 2021. Improving forest above ground biomass estimates over Indian forests using multi source data sets with machine learning algorithm. *Ecol. Inform.* 65, 101392 <https://doi.org/10.1101/j.ecoinf.2021.101392>.
- Fayad, I., Baghdadi, N., Baily, J.S., Barbier, N., Gond, V., Héroult, B., el Hajj, M., Fabre, F., Perrin, J., 2016. Regional scale rain-forest height mapping using regression-kriging of spaceborne and airborne LiDAR data: application on French Guiana. *Remote Sens.* 8, 240. <https://doi.org/10.3390/rs8030240>.
- Freitas, S.R., Mello, M.C.S., Cruz, C.B.M., 2005. Relationships between forest structure and vegetation indices in Atlantic rainforest. *For. Ecol. Manag.* 218, 353–362. <https://doi.org/10.1016/j.foreco.2005.08.036>.
- FSI (Forest Survey of India), 1996. Volume Equations for Forests of India, Nepal and Bhutan.
- Ghasemi, N., Reza Sahebi, M., Mohammadzadeh, A., 2011. A review on biomass estimation methods using synthetic aperture radar data. *Int. J. Geomat. Geosci.* 1, 776–788.
- Gibbs, H.K., Brown, S., Niles, J.O., Foley, J.A., 2007. Monitoring and estimating tropical forest carbon stocks: making REDD a reality. *Environ. Res. Lett.* 2, 045023 <https://doi.org/10.1088/1748-9326/2/4/045023>.
- Gupta, R., Sharma, L.K., 2022. Mixed tropical forests canopy height mapping from spaceborne LiDAR GEDI and multisensor imagery using machine learning models. *Remote Sens. Appl.: Soc. Environ.* 27, 100817 <https://doi.org/10.1016/j.rsase.2022.100817>.
- Hajnsek, I., Kugler, F., Lee, S.K., Papathanassiou, K.P., 2009. Tropical-forest-parameter estimation by means of pol-InSAR: the INDREX-II campaign. *IEEE Trans. Geosci. Remote Sens.* 47, 481–493. <https://doi.org/10.1109/TGRS.2008.2009437>.
- Hall, F.G., Bergen, K., Blair, J.B., Dubayah, R., Houghton, R., Hurt, G., Kellndorfer, J., Lefsky, M., Ranson, J., Saatchi, S., Shugart, H.H., Wickland, D., 2011. Characterizing 3D vegetation structure from space: Mission requirements. *Remote Sens. Environ.* 115, 2753–2775. <https://doi.org/10.1016/j.rse.2011.01.024>.
- Hancock, S., Armston, J., Hofton, M., Sun, X., Tang, H., Duncanson, L., Kellner, J., Dubayah, R., 2019. The Gedi simulator: a large-footprint waveform lidar simulator for calibration and validation of spaceborne missions. *Earth Space Sci.* 6, 294–310. <https://doi.org/10.1029/2018EA000506>.
- Hansen, M.C., Potapov, P.V., Moore, R., Hancher, M., Turubanova, S.A., Tyukavina, A., Thau, D., Stehman, S.V., Goetz, S.J., Loveland, T.R., Kommareddy, A., 2013. High-resolution global maps of 21st-century forest cover change. *Sci.* 342 (6160), 850–853. <https://doi.org/10.1126/science.1244693>.
- Hansen, M.C., Potapov, P.V., Goetz, S.J., Turubanova, S., Tyukavina, A., Krylov, A., Kommareddy, A., Egorov, A., 2016. Mapping tree height distributions in sub-Saharan Africa using Landsat 7 and 8 data. *Remote Sens. Environ.* 185, 221–232. <https://doi.org/10.1016/j.rse.2016.02.023>.
- Harding, D.J., Lefsky, M.A., Parker, G.G., Blair, J.B., 2001. Laser altimeter canopy height profiles methods and validation for closed-canopy, broadleaf forests. *Remote Sens. Environ.* 76, 283–297. [https://doi.org/10.1016/S0034-4257\(00\)00210-8](https://doi.org/10.1016/S0034-4257(00)00210-8).
- Healey, S.P., Yang, Z., Gorelick, N., Ilyushchenko, S., 2020. Highly local model calibration with a new GEDI LiDAR asset on google earth engine reduces landsat forest height signal saturation. *Remote Sens. Environ.* 12, 2840. <https://doi.org/10.3390/rs12172840>.
- Herold, M., Carter, S., Avitabile, V., Espejo, A.B., Jonckheere, I., Lucas, R., McRoberts, R. E., Næsset, E., Nightingale, J., Petersen, R., Reiche, J., Romijn, E., Rosenqvist, A., Rozendaal, D.M.A., Seifert, F.M., Sanz, M.J., de Sy, V., 2019. The role and need for space-based Forest biomass-related measurements in environmental management and policy. *Surv. Geophys.* 40, 757–778. <https://doi.org/10.1007/s10712-019-09510-6>.
- Hojo, A., Avatar, R., Nakaji, T., Tadono, T., Takagi, K., 2023. Modeling forest above-ground biomass using freely available satellite and multisource datasets. *Ecol. Inform.* 101973 <https://doi.org/10.1016/j.ecoinf.2023.101973>.
- Houghton, R.A., Hall, F., Goetz, S.J., 2009. Importance of biomass in the global carbon cycle. *J. Geophys. Res. Biogeosci.* 114 <https://doi.org/10.1029/2009JG000935>.
- Huete, A., Didan, K., Miura, T., Rodriguez, E.P., Gao, X., Ferreira, L.G., 2002. Overview of the radiometric and biophysical performance of the MODIS vegetation indices. *Remote Sens. Environ.* 83, 195–213. [https://doi.org/10.1016/S0034-4257\(02\)00096-2](https://doi.org/10.1016/S0034-4257(02)00096-2).
- Hunter, M.O., Keller, M., Vitoria, D., Morton, D.C., 2013. Tree height and tropical forest biomass estimation. *Biogeosciences* 10, 8385–8399. <https://doi.org/10.5194/bg-10-10491-2013>.
- Hyde, P., Dubayah, R., Walker, W., Blair, J.B., Hofton, M., Hunsaker, C., 2006. Mapping forest structure for wildlife habitat analysis using multi-sensor (LiDAR, SAR/InSAR, ETM+, Quickbird) synergy. *Remote Sens. Environ.* 102, 63–73. <https://doi.org/10.1016/j.rse.2006.01.021>.
- Hyppä, J., Hyppä, E.H., Inkinen, M., Engdahl, M., Linko, S., Zhu, Y.-H., 2000. Accuracy comparison of various remote sensing data sources in the retrieval of forest stand attributes. *For. Ecol. Manag.* 128, 109–120. [https://doi.org/10.1016/S0378-1127\(99\)00278-9](https://doi.org/10.1016/S0378-1127(99)00278-9).
- Karabulut, M., Küçükönder, M., 2019. An examination of temporal changes in Göksu Delta (Turkey) using principle component analysis. *Intern. J. Geogr. Geogr. Educ.* 39, 279–299.
- Kasischke, E.S., Melack, J.M., Dobson, M.C., 1997. The use of imaging radars for applications a review. *Remote Sens. Environ.* 59, 141–156. [https://doi.org/10.1016/S0034-4257\(96\)00148-4](https://doi.org/10.1016/S0034-4257(96)00148-4).
- Khati, U., Lavalle, M., Singh, G., 2021. The role of time-series L-band SAR and GEDI in mapping sub-tropical above-ground biomass. *Front. Earth Sci.* 9, 752254 <https://doi.org/10.3389/feart.2021.752254>.
- Kilpeläinen, P., Tokola, T., 1999. Gain to be achieved from stand delineation in LANDSAT TM image-based estimates of stand volume. *For. Ecol. Manag.* 124, 105–111. [https://doi.org/10.1016/S0378-1127\(99\)00059-6](https://doi.org/10.1016/S0378-1127(99)00059-6).
- Kugler, F., Lee, S.K., Hajnsek, I., Papathanassiou, K.P., 2015. Forest height estimation by means of pol-InSAR data inversion: the role of the vertical wavenumber. *IEEE Trans. Geosci. Remote Sens.* 53, 5294–5311. <https://doi.org/10.1109/TGRS.2015.2420996>.
- Kumar, S., Pandey, U., Kushwaha, S.P., Chatterjee, R.S., Bijker, W., 2012. Aboveground biomass estimation of tropical forest from Envisat advanced synthetic aperture radar data using modeling approach. *J. Appl. Remote. Sens.* 6, 063588 <https://doi.org/10.1117/1.jrs.6.063588>.
- Kurvonnen, L., Pulliainen, J., Hallikainen, M., 1999. Retrieval of biomass in boreal forests from multitemporal ERS-1 and JERS-1 SAR images. *IEEE Trans. Geosci. Remote Sens.* 37, 198–205. <https://doi.org/10.1109/36.739154>.
- Lang, N., Schindler, K., Wegner, J.D., 2021. High carbon stock mapping at large scale with optical satellite imagery and spaceborne LiDAR arXiv preprint arXiv: 2107.07431.
- Lang, N., Kalischek, N., Armston, J., Schindler, K., Dubayah, R., Wegner, R., 2022. Global canopy height regression and uncertainty estimation from GEDI LiDAR waveforms with deep ensembles. *Remote Sens. Environ.* 268, 112760 <https://doi.org/10.1016/j.rse.2021.112760>.
- Lausch, A., Erasmi, S., King, D.J., Magdon, P., Heurich, M., 2017. Understanding forest health with remote sensing-part II-A review of approaches and data models. *Remote Sens.* 9, 129. <https://doi.org/10.3390/rs9020129>.
- Lefsky, M.A., 2010. A global forest canopy height map from the moderate resolution imaging spectroradiometer and the geoscience laser altimeter system. *Geophys. Res. Lett.* 37 <https://doi.org/10.1029/2010GL043622>.
- Lefsky, M.A., Cohen, W.B., Harding, D.J., Parker, G.G., Acker, S.A., Gower, S.T., 2002. Lidar remote sensing of above-ground biomass in three biomes. *Glob. Ecol. Biogeogr.* 11, 393–399. <https://doi.org/10.1046/j.1466-822x.2002.00303.x>.
- Lehmann, E.A., Caccetta, P., Lowell, K., Mitchell, A., Zhou, Z.S., Held, A., Milne, T., Tapley, I., 2015. SAR and optical remote sensing: assessment of complementarity and interoperability in the context of a large-scale operational forest monitoring system. *Remote Sens. Environ.* 156, 335–348. <https://doi.org/10.1016/j.rse.2014.09.034>.
- Li, Y., Li, M., Li, C., Liu, Z., 2020. Forest aboveground biomass estimation using Landsat 8 and sentinel-1A data with machine learning algorithms. *Sci. Rep.* 10 <https://doi.org/10.1038/s41598-020-67024-3>.
- Liang, M., Duncanson, L., Silva, J.A., Sedano, F., 2023. Quantifying aboveground biomass dynamics from charcoal degradation in Mozambique using GEDI Lidar and Landsat. *Remote Sens. Environ.* 284, 113367 <https://doi.org/10.1016/j.rse.2022.113367>.
- López-Serrano, P.M., Domínguez, J.L.C., Corral-Rivas, J.J., Jiménez, E., López-Sánchez, C.A., Vega-Nieva, D.J., 2020. Modeling of aboveground biomass with Landsat 8 OLI and machine learning in temperate forests. *Forests* 11, 11. <https://doi.org/10.3390/f11010011>.
- Loveland, R.T., Irons, R.J., 2016. Landsat 8: the plans, the reality, and the legacy. *Remote Sens. Environ.* 185, 1–6. <https://doi.org/10.1016/j.rse.2016.07.033>.
- Lu, D., 2005. Aboveground biomass estimation using Landsat TM data in the Brazilian Amazon. *Int. J. Remote Sens.* 26, 2509–2525. <https://doi.org/10.1080/0143160500142145>.
- Lucas, R., Bunting, P., Clewley, D., Armston, J., Fairfax, R., Fensham, R., Accad, A., Kelley, J., Laidlow, M., Eyre, T., Bowen, M., Carreiras, J., Bray, S., Metcalfe, D., Dwyer, J., Shimada, M., 2010. An evaluation of the ALOS PALSAR L-band backscatter—above ground biomass relationship Queensland, Australia: impacts of surface moisture condition and vegetation structure. *IEEE J. Sel. Top. Appl. Earth Obs. Remote Sens.* 3, 576–593. <https://doi.org/10.1109/JSTARS.2010.2086436>.
- Lucas, R.M., Moghaddam, M., Cronin, N., 2004. Microwave scattering from mixed-species forests, Queensland, Australia. *IEEE Trans. Geosci. Remote Sens.* 42, 2142–2159. <https://doi.org/10.1109/TGRS.2004.834633>.
- Lucas, R.M., Cronin, N., Lee, A., Moghaddam, M., Witte, C., Tickle, P., 2006. Empirical relationships between AIRSAR backscatter and LiDAR-derived forest biomass, Queensland, Australia. *Remote Sens. Environ.* 100, 407–425. <https://doi.org/10.1016/j.rse.2005.10.019>.
- Luthcke, S., Rebold, T., Thomas, T., Pennington, T., 2019. Algorithm Theoretical Basis Document (ATBD) for GEDI Waveform Geolocation for L1 and L2 Products.
- Masek, J.G., Hayes, D.J., Joseph Hughes, M., Healey, S.P., Turner, D.P., 2015. The role of remote sensing in process-scaling studies of managed forest ecosystems. *For. Ecol. Manag.* 355, 109–123. <https://doi.org/10.1016/j.foreco.2015.05.032>.
- Mauya, E.W., Hansen, E.H., Gobakken, T., Bollandsås, O.M., Malimbwi, R.E., Næsset, E., 2015. Effects of field plot size on prediction accuracy of aboveground biomass in airborne laser scanning-assisted inventories in tropical rain forests of Tanzania. *Carbon Balance Manag.* 10 <https://doi.org/10.1186/s13021-015-0021-x>.
- Mauya, E.W., Koskinen, J., Tegel, K., Hämaläinen, J., Kauranne, T., Käyhkö, N., 2019. Modelling and predicting the growing stock volume in small-scale plantation forests of tanzania using multi-sensor image synergy. *Forests* 10, 279. <https://doi.org/10.3390/f10030279>.
- Mette, T., Papathanassiou, K., Hajnsek, I., 2004. Biomass estimation from polarimetric SAR interferometry over heterogeneous forest terrain. In: IGARSS 2004. 2004 IEEE

- International Geoscience and Remote Sensing Symposium 1, 511–514. <https://doi.org/10.1109/IGARSS.2004.1369076>.
- Mitchard, E.T., Saatchi, S.S., Baccini, A., Asner, G.P., Goetz, S.J., Harris, N.L., Brown, S., 2013. Uncertainty in the spatial distribution of tropical forest biomass: a comparison of pan-tropical maps. *Carbon Bal. Manage.* 8, 1–13. <https://doi.org/10.1186/1750-0680-8-10>.
- Mitchard, E.T.A., Saatchi, S.S., Woodhouse, I.H., Nangendo, G., Ribeiro, N.S., Williams, M., Ryan, C.M., Lewis, S.L., Feldpausch, T.R., Meir, P., 2009. Using satellite radar backscatter to predict above-ground woody biomass: a consistent relationship across four different African landscapes. *Geophys. Res. Lett.* 36 <https://doi.org/10.1029/2009GL040692>.
- Mitchard, E.T.A., Saatchi, S.S., White, L.J.T., Abernethy, K.A., Jeffery, K.J., Lewis, S.L., Collins, M., Lefsky, M.A., Leal, M.E., Woodhouse, I.H., Meir, P., 2012. Mapping tropical forest biomass with radar and spaceborne LiDAR in Lopé National Park, Gabon: overcoming problems of high biomass and persistent cloud. *Biogeosci.* 9, 179–191. <https://doi.org/10.5194/bg-9-179-2012>.
- Montesano, P.M., Nelson, R.F., Dubayah, R.O., Sun, G., Cook, B.D., Ranson, K.J.R., Næsset, E., Kharuk, V., 2014. The uncertainty of biomass estimates from LiDAR and SAR across a boreal forest structure gradient. *Remote Sens. Environ.* 154, 398–407. <https://doi.org/10.1016/j.rse.2014.01.027>.
- Nandy, S., Srinet, R., Padalia, H., 2021. Mapping forest height and aboveground biomass by integrating icesat-2, Sentinel-1 and sentinel-2 data using random forest algorithm in northwest Himalayan foothills of India. *Geophys. Res. Lett.* 48 <https://doi.org/10.1029/2021GL093799>.
- Narine, L.L., Popescu, S.C., Malambo, L., 2020. Using ICESat-2 to estimate and map forest aboveground biomass: a first example. *Remote Sens.* 12, 1824. <https://doi.org/10.3390/rs12111824>.
- Nguyen, L.V., Van Nguyen, H., Kieu, L.Q., To, T. T., Phan, T.K.T., Pham, T.A., Tran, C.K., 2020. Seasonal effects of backscattering intensity of ALOS-2 PALSAR-2 (L-band) on retrieval forest biomass in the tropics. *J. Geosci. Enviro. Pro.* 8 (11), 26–40. <https://doi.org/10.4236/gep.2020.811002>.
- Ni-Meister, W., Rojas, A., Lee, S., 2022. Direct use of large-footprint lidar waveforms to estimate aboveground biomass. *Remote Sens. Environ.* 280, 113147 <https://doi.org/10.1016/j.rse.2022.113147>.
- NISAR Science Team, 2019. NASA-ISRO SAR Mission Science Users Handbook. Available online: [https://nisar.jpl.nasa.gov/files/nisar/NISAR\\_Science\\_Users\\_Handbook.pdf](https://nisar.jpl.nasa.gov/files/nisar/NISAR_Science_Users_Handbook.pdf).
- Olesk, A., Praks, J., Antropov, O., Zalite, K., Arumäe, T., Voormansik, K., 2016. Interferometric SAR coherence models for characterization of hemiboreal forests using TanDEM-X dssata. *Remote Sens.* 8, 700. <https://doi.org/10.3390/rs8090700>.
- Padalia, H., Yadav, S., 2016. Evaluation of RISAT-1 SAR data for tropical forestry applications. *Adv. Space Res.* 59, 2–11. <https://doi.org/10.1016/j.asr.2016.08.026>.
- Pascual, A., Tupinambá-Simões, F., de Conto, T., 2022. Using multi-temporal tree inventory data in eucalypt forestry to benchmark global high-resolution canopy height models. A showcase in Mato Grosso, Brazil. *Ecol. Inform.* 70, 101748 <https://doi.org/10.1016/j.ecoinf.2022.101748>.
- Popescu, S.C., Zhao, K., Neuenschwander, A., Lin, C., 2011. Satellite lidar vs. small footprint airborne lidar: comparing the accuracy of aboveground biomass estimates and forest structure metrics at footprint level. *Remote Sens. Environ.* 115, 2786–2797. <https://doi.org/10.1016/j.rse.2011.01.026>.
- Popatov, P., Li, X., Hernandez-Serna, A., Tyukavina, A., Hansen, M.C., Kommareddy, A., Pickens, A., Turubanova, S., Tang, H., Silva, C.E., Armstrong, J., Dubayah, R., Blair, J. B., Hofton, M., 2021. Mapping global forest canopy height through integration of GEDI and Landsat data. *Remote Sens. Environ.* 253, 112165 <https://doi.org/10.1016/j.rse.2020.112165>.
- Prakash, A.J., Behera, M.D., Ghosh, S.M., Das, A., Mishra, D.R., 2022. A new synergistic approach for Sentinel-1 and PALSAR-2 in a machine learning framework to predict aboveground biomass of a dense mangrove forest. *Ecol. Inform.* 72, 101900 <https://doi.org/10.1016/j.ecoinf.2022.101900>.
- Puliti, S., Saarela, S., Gobakken, T., Ståhl, G., Næsset, E., 2018. Combining UAV and Sentinel-2 auxiliary data for forest growing stock volume estimation through hierarchical model-based inference. *Remote Sens. Environ.* 204, 485–497.
- Pulliajainen, J.T., Kurvonen, L., Hallikainen, M.T., 1999. Multitemporal behavior of L-and C-band SAR observations of boreal forests. *IEEE Trans. Geosci. Remote Sens.* 37, 927–937. <https://doi.org/10.1109/36.752211>.
- Qi, W., Saarela, S., Armstrong, J., Ståhl, G., Dubayah, R., 2019. Forest biomass estimation over three distinct forest types using TanDEM-X InSAR data and simulated GEDI lidar data. *Remote Sens. Environ.* 232, 111283 <https://doi.org/10.1016/j.rse.2019.111283>.
- Rauste, Y., 2005. Multi-temporal JERS SAR data in boreal forest biomass mapping. *Remote Sens. Environ.* 97, 263–275. <https://doi.org/10.1016/j.rse.2005.05.002>.
- Réjou-Méchain, M., Barbier, N., Couteron, P., Ploton, P., Vincent, G., Herold, M., Mermoz, S., Saatchi, S., Chave, J., de Boissieu, F., Féret, J.B., Takoudjou, S.M., Pélassier, R., 2019. Upscaling Forest biomass from field to satellite measurements: sources of errors and ways to reduce them. *Surv. Geophys.* 40, 881–911. <https://doi.org/10.1007/s10712-019-09532-0>.
- Rikimaru, A., Roy, P.S., Miyatake, S., 2002. Tropical forest cover density mapping. *Trop. Ecol.* 43 (1), 39–47.
- Roy, D.P., Kashongwe, H.B., Armstrong, J., 2021. The impact of geolocation uncertainty on GEDI tropical forest canopy height estimation and change monitoring. *Sci. Remote Sens.* 4, 100024 <https://doi.org/10.1016/j.srs.2021.100024>.
- Saatchi, S., 2019. SAR methods for mapping and monitoring Forest biomass. In: Flores, A., Herndon, K., Thapa, R., Cherrington, E. (Eds.), *SAR Handbook: Comprehensive Methodologies for Forest Monitoring and Biomass Estimation*, pp. 207–246.
- Saatchi, S., Marlier, M., Chazdon, R.L., Clark, D.B., Russell, A.E., 2011. Impact of spatial variability of tropical forest structure on radar estimation of aboveground biomass. *Remote Sens. Environ.* 115 (11), 2836–2849.
- Santi, E., Paloscia, S., Pettinato, S., Chirici, G., Mura, M., Maselli, F., 2015. Application of neural networks for the retrieval of forest woody volume from SAR multifrequency data at L and C bands. *Eur. J. Remote Sens.* 48, 673–687. <https://doi.org/10.5721/EuJRS20154837>.
- Santoro, M., 2003. *Estimation of Biophysical Parameters in Boreal Forests from ERS and JERS SAR Interferometry*. PhD diss. Department of Radio and Space Science, Chalmers University of Technology.
- Santoro, M., Cartus, O., 2018. Research pathways of forest above-ground biomass estimation based on SAR backscatter and interferometric SAR observations. *Remote Sens.* 10, 608. <https://doi.org/10.3390/rs10040608>.
- Santoro, M., Askne, J., Dammert, P.B.G., Fransson, J.E.S., Smith, G., 1999. Retrieval of biomass in boreal Forest from multi-temporal ERS-1/2 interferometry. *Image* 21, 55.
- Santoro, M., Askne, J., Smith, G., Fransson, J.E.S., 2002. Stem volume retrieval in boreal forests from ERS-1/2 interferometry. *Remote Sens. Environ.* 81, 19–35. [https://doi.org/10.1016/S0034-4257\(01\)00329-7](https://doi.org/10.1016/S0034-4257(01)00329-7).
- Santoro, M., Eriksson, L.E.B., Fransson, J.E.S., 2015. Reviewing ALOS PALSAR backscatter observations for stem volume retrieval in Swedish forest. *Remote Sens.* 7, 4290–4317. <https://doi.org/10.3390/rs70404290>.
- Schildhauer, M., 2018. Data integration: principles and practice. *Ecol. Inform.: Data Manage. Knowledg. Discov.* 129–157 <https://doi.org/10.1007/978-3-319-59928-1>.
- Shendryk, Y., 2022. Fusing GEDI with earth observation data for large area aboveground biomass mapping. *Int. J. Appl. Earth Obs. Geoinf.* 115, 103108 <https://doi.org/10.1016/j.jag.2022.103108>.
- Simard, M., Pinto, N., Fisher, J.B., Baccini, A., 2011. Mapping forest canopy height globally with spaceborne LiDAR. *J. Geophys. Res.* 116 <https://doi.org/10.1029/2011JG001708>.
- Staben, G., Lucieer, A., Scarth, P., 2018. Modelling LiDAR derived tree canopy height from Landsat TM, ETM+ and OLI satellite imagery-a machine learning approach. *Int. J. Appl. Earth Obs. Geoinf.* 73, 666–681. <https://doi.org/10.1016/j.jag.2018.08.013>.
- Sun, M., Cui, L., Park, J., García, M., Zhou, Y., Silva, C.A., He, L., Zhang, H., Zhao, K., 2022. Evaluation of NASA's GEDI Lidar observations for estimating biomass in temperate and tropical forests. *Forests* 13, 1686. <https://doi.org/10.3390/f13101686>.
- Tanase, M.A., Panciera, R., Lowell, K., Tian, S., Hacker, J.M., Walker, J.P., 2014. Airborne multi-temporal L-band polarimetric SAR data for biomass estimation in semi-arid forests. *Remote Sens. Environ.* 145, 93–104. <https://doi.org/10.1016/j.rse.2014.01.024>.
- Thiel, C., Schmullius, C., 2016. The potential of ALOS PALSAR backscatter and InSAR coherence for forest growing stock volume estimation in Central Siberia. *Remote Sens. Environ.* 173, 258–273. <https://doi.org/10.1016/j.rse.2015.10.030>.
- Thumay, K.C., Fararoda, R., Middinti, S., Gopalakrishnan, R., Jha, C.S., Dadhwali, V.K., 2016. Estimation of above ground biomass for central Indian deciduous forests using ALOS PALSAR L-band data. *J. Indian Soc. Remote Sens.* 44 (1), 31–39.
- Torresani, M., Rocchini, D., Alberti, A., Moudrá, V., Heym, M., Thouverai, E., Kacic, P., Tomelleri, E., 2023. LiDAR GEDI derived tree canopy height heterogeneity reveals patterns of biodiversity in forest ecosystems. *Ecol. Inform.* 76, 102082 <https://doi.org/10.1016/j.ecoinf.2023.102082>.
- Uttarakhand forest Department, 2016. *Working Plan, 2015–2016. Tarai Central Forest Division, Haldwani. Govt. of Uttarakhand, India*.
- Vafaei, S., Soosani, J., Adeli, K., Fadaei, H., Naghavi, H., Pham, T.D., Bui, D.T., 2018. Improving accuracy estimation of Forest aboveground biomass based on incorporation of ALOS-2 PALSAR-2 and sentinel-2A imagery and machine learning: a case study of the Hyrcanian forest area (Iran). *Remote Sens.* 10, 172. <https://doi.org/10.3390/rs10020172>.
- Wang, C., Elmore, A.J., Numata, I., Cochrane, M.A., Shaogang, L., Huang, J., Zhao, Y., Li, Y., 2022. Factors affecting relative height and ground elevation estimations of GEDI among forest types across the conterminous USA. *Glaci. Remote Sens.* 59, 975–999. <https://doi.org/10.1080/15481603.2022.2085354>.
- Wang, L., Jia, M., Yin, D., Tian, J., 2018. A review of remote sensing for mangrove forests: 1956–2018. *Remote Sens. Environ.* 231, 111223 <https://doi.org/10.1016/j.rse.2019.111223>.
- Watanabe, M., Shimada, M., Rosenqvist, A., Tadono, T., Matsuoka, M., Romshoo, S.A., Ohta, K., Furuta, R., Nakamura, K., Moriyama, T., 2006. Forest structure dependency of the relation between L-band σ 0 and biophysical parameters. *IEEE Trans. Geosci. Remote Sens.* 44, 3154–3164. <https://doi.org/10.1109/TGRS.2006.880632>.
- Watham, T., Padalia, H., Srinet, R., Nandy, S., Verma, P.A., Chauhan, P., 2021. Seasonal dynamics and impact factors of atmospheric CO2 concentration over subtropical forest canopies: observation from eddy covariance tower and OCO-2 satellite in northwest Himalaya, India. *Environ. Monit. Assess.* 193 <https://doi.org/10.1007/s10661-021-08896-4>.
- Way, D.A., Pearcey, R.W., 2012. Sunflecks in trees and forests: from photosynthetic physiology to global change biology. *Tree Physiol.* 32, 1066–1081. <https://doi.org/10.1093/treephys/tps064>.
- Wu, C., Shen, H., Wang, K., Shen, A., Deng, J., Gan, M., 2016. Landsat imagery-based above ground biomass estimation and change investigation related to human activities. *Sustainability* 8, 159. <https://doi.org/10.3390/su8020159>.
- Yadav, S., Padalia, H., Sinha, S.K., Srinet, R., Chauhan, P., 2021. Above-ground biomass estimation of Indian tropical forests using X band pol-InSAR and random forest. *Remote Sens. Appl.: Soc. Environ.* 21, 100462 <https://doi.org/10.1016/j.rsase.2020.100462>.

- Yu, Y., Saatchi, S., 2016. Sensitivity of L-band SAR backscatter to aboveground biomass of global forests. *Remote Sens.* 8, 522. <https://doi.org/10.3390/rs8060522>.
- Zhang, Y., Ma, J., Liang, S., Li, X., Li, M., 2020. An evaluation of eight machine learning regression algorithms for forest aboveground biomass estimation from multiple satellite data products. *Remote Sens.* 12, 4015. <https://doi.org/10.3390/rs12244015>.
- Zheng, D., Rademacher, J., Chen, J., Crow, T., Bresee, M., le Moine, J., Ryu, S.R., 2004. Estimating aboveground biomass using Landsat 7 ETM+ data across a managed landscape in northern Wisconsin, USA. *Remote Sens. Environ.* 93, 402–411. <https://doi.org/10.1016/j.rse.2004.08.008>.